



Article

Remote Sensing Supported Sea Surface pCO₂ Estimation and Variable Analysis in the Baltic Sea

Shuping Zhang ^{1,*}, Anna Rutgersson ¹ , Petra Philipson ² and Marcus B. Wallin ^{1,3}

¹ Department of Earth Sciences, Uppsala University, SE-752 36 Uppsala, Sweden; Anna.Rutgersson@met.uu.se (A.R.); Marcus.Wallin@slu.se (M.B.W.)

² Brockmann Geomatics Sweden AB, SE-164 40 Kista, Sweden; petra.philipson@brockmann-geomatics.se

³ Department of Aquatic Sciences and Assessment, Swedish University of Agricultural Sciences, SE-750 07 Uppsala, Sweden

* Correspondence: shuping.zhang@geo.uu.se

Abstract: Marginal seas are a dynamic and still to large extent uncertain component of the global carbon cycle. The large temporal and spatial variations of sea-surface partial pressure of carbon dioxide (pCO₂) in these areas are driven by multiple complex mechanisms. In this study, we analyzed the variable importance for the sea surface pCO₂ estimation in the Baltic Sea and derived monthly pCO₂ maps for the marginal sea during the period of July 2002–October 2011. We used variables obtained from remote sensing images and numerical models. The random forest algorithm was employed to construct regression models for pCO₂ estimation and produce the importance of different input variables. The study found that photosynthetically available radiation (PAR) was the most important variable for the pCO₂ estimation across the entire Baltic Sea, followed by sea surface temperature (SST), absorption of colored dissolved organic matter (a_{CDOM}), and mixed layer depth (MLD). Interestingly, Chlorophyll-a concentration (Chl-a) and the diffuse attenuation coefficient for downwelling irradiance at 490 nm (K_{d_490nm}) showed relatively low importance for the pCO₂ estimation. This was mainly attributed to the high correlation of Chl-a and K_{d_490nm} to other pCO₂-relevant variables (e.g., a_{CDOM}), particularly in the summer months. In addition, the variables' importance for pCO₂ estimation varied between seasons and sub-basins. For example, the importance of a_{CDOM} were large in the Gulf of Finland but marginal in other sub-basins. The model for pCO₂ estimate in the entire Baltic Sea explained 63% of the variation and had a root of mean squared error (RMSE) of 47.8 μatm. The pCO₂ maps derived with this model displayed realistic seasonal variations and spatial features of sea surface pCO₂ in the Baltic Sea. The spatially and seasonally varying variables' importance for the pCO₂ estimation shed light on the heterogeneities in the biogeochemical and physical processes driving the carbon cycling in the Baltic Sea and can serve as an important basis for future pCO₂ estimation in marginal seas using remote sensing techniques. The pCO₂ maps derived in this study provided a robust benchmark for understanding the spatiotemporal patterns of CO₂ air-sea exchange in the Baltic Sea.

Keywords: pCO₂; remote sensing; random forest; variable importance; the Baltic Sea



Citation: Zhang, S.; Rutgersson, A.; Philipson, P.; Wallin, M.B. Remote Sensing Supported Sea Surface pCO₂ Estimation and Variable Analysis in the Baltic Sea. *Remote Sens.* **2021**, *13*, 259. <https://doi.org/10.3390/rs13020259>

Received: 19 November 2020

Accepted: 12 January 2021

Published: 13 January 2021

Publisher's Note: MDPI stays neutral with regard to jurisdictional claims in published maps and institutional affiliations.



Copyright: © 2021 by the authors. Licensee MDPI, Basel, Switzerland. This article is an open access article distributed under the terms and conditions of the Creative Commons Attribution (CC BY) license (<https://creativecommons.org/licenses/by/4.0/>).

1. Introduction

Global oceans are an important sink of atmospheric CO₂ and uptake approximately 30% of the global anthropogenic CO₂ emissions [1]. As the global ocean uptake of CO₂ increases by a rate proportional to the atmospheric CO₂, substantial differences exist between oceans and marginal seas [1,2]. The changing air-sea exchange of CO₂ in marginal seas, particularly those at high-latitude, is found to be the major source of uncertainties in the estimate of ocean CO₂ uptake [3,4]. As the atmospheric CO₂ is as rather globally homogeneous, sea surface partial pressure of carbon dioxide (pCO₂) in the marginal sea is the key component for precisely determining the direction of the air-sea exchange of CO₂.

Therefore, deriving maps of the changing $p\text{CO}_2$ for marginal seas over time is critical for precise estimate of global air-sea exchange and ocean uptake of CO_2 [2,3,5].

Generally, sea surface $p\text{CO}_2$ is jointly determined by biogeochemical processes, vertical and horizontal mixing of sea water, and the air-sea exchange of CO_2 [6,7]. Many sea surface variables related to these processes are can be retrieved from remote sensing images. Given their vast spatial coverages, remotely sensed sea surface variables have increasingly been used in sea surface $p\text{CO}_2$ estimation. Remotely sensed Chlorophyll-a concentration (Chl-a) is commonly used as an indicator of biological activities in water [8]. Sea surface temperature (SST) largely determines the solubility of CO_2 in sea water and has been frequently used to estimate $p\text{CO}_2$ from remote sensing [9–13]. In addition, bacteria respiration produces CO_2 by decomposing dissolved organic matter (DOM) [14,15]. Therefore, absorption of colored dissolved organic matter (aCDOM) retrieved from remote sensing images was used in sea surface $p\text{CO}_2$ estimation [16,17]. Furthermore, after [18] found from in-situ measurements that sea surface salinity (SSS) was highly related to sea surface $p\text{CO}_2$, SSS derived directly from remote sensing images or remotely sensed aCDOM were adopted to support sea surface $p\text{CO}_2$ estimate [16,19]. $K_d_{490\text{nm}}$, a proxy of water transparency, was derived from remote sensing and included in sea surface $p\text{CO}_2$ estimation to indicate the effect of biological activities [16]. Mixed layer depth (MLD) determines thermal stratification between different water masses and, however, is not retrievable with remote sensing approaches. Therefore, some studies used the MLD obtained from ocean models to support the derivation of sea surface $p\text{CO}_2$ maps [9,12]. Similarly, model-yield gross primary production (GPP) and net primary production (NPP) were also included to support $p\text{CO}_2$ estimation by approximating the biological control on $p\text{CO}_2$ in sea water [9,12].

Sea surface $p\text{CO}_2$ in many global marginal seas have been estimated with various remote sensing supported approaches [9,12,16,17,20–23]. Most of the studies chose the variables based on empirical knowledge and focused on deriving $p\text{CO}_2$ maps with small estimate errors (e.g., RMSE). However, few studies have investigated the spatiotemporal variabilities of the variable's relevance to sea surface $p\text{CO}_2$ in marginal seas. Considering the high spatial variabilities in the controlling forces of sea surface $p\text{CO}_2$ in marginal seas, some studies divided the targeted seas into sub-basins/subsets and separately constructed models for $p\text{CO}_2$ retrieval in each of the sub-basins/subset [12,22,24]. Though this strategy produced maps of good quality in the sub-basins/subsets, it provided little knowledge on the variables' relevance to $p\text{CO}_2$ distribution. Furthermore, Reference [25] regarded the sea surface $p\text{CO}_2$ in the targeted area as a mixture of the $p\text{CO}_2$ controlled by different processes (e.g., vertical mixing and biological uptake) and determined each of the processes separately from different sets of variables. Despite the successfully applications in multiple marginal seas [10,25,26], their method was often limited to $p\text{CO}_2$ estimation in summer time and thus fails to provide information for other seasons. Overall, large space remains for investigation on variables' relevance (importance) in sea surface $p\text{CO}_2$ estimate across different time and space.

The Baltic Sea is a semi-enclosed marginal sea located in northern Europe. The carbon budget of the Baltic Sea displays considerable seasonal and interannual variabilities. To date, the few studies attempting to estimate sea surface $p\text{CO}_2$ in the Baltic Sea using remote sensing approaches, e.g., [12], have barely provided information on the variables' relevance/importance to the $p\text{CO}_2$ estimate for this marginal sea. In this study, we aimed to analyze the importance of different variables for $p\text{CO}_2$ estimation and derive improved monthly $p\text{CO}_2$ maps for the Baltic Sea from 2002 to 2011. We conducted the following: (1) filtering the in-situ $p\text{CO}_2$ data for the model training and validation; (2) assessing the relative importance of the input variables for the $p\text{CO}_2$ estimation on different spatial and seasonal scales; and (3) deriving $p\text{CO}_2$ maps for the Baltic Sea.

2. Study Area

The Baltic Sea is located at high latitudes (55–60° N) in Europe. As the sun illumination and temperature there exhibit significant seasonal changes, the Baltic Sea and adjacent

terrestrial ecosystems also undergo high seasonality. In addition, the wide span of the Baltic Sea in latitude forms a large spatial gradient in sun illumination and the corresponding environment condition, like SST. The Baltic Sea has restricted water exchange with the open North Atlantic Ocean via the Danish straits and is a semi-enclosed marginal sea. More than 600 rivers drain the catchment of total 1.7 million km² and export to the Baltic Sea substantial freshwater and terrigenous substances, including organic carbon [27–30]. Therefore, the Baltic Sea is characterized with a high concentration of CDOM, and most part of the sea presents as “brown water”. With varying inputs from different rivers, the sub-basins of the Baltic Sea create highly heterogeneous biogeochemical conditions in this marginal sea. Consequently, the pCO₂ distribution in the Baltic Sea displays evident seasonality and spatial heterogeneity [31]. Upwelling characterized with evident seasonality and spatiality occurs frequently in the Baltic Sea and brings up deep water of high pCO₂ up to 2000 µatm to the sea surface [32,33]. The high concentration of nutrients brought up together with the deep water leads to cyanobacteria and phytoplankton blooms after the upwelling event, which further complicates the pCO₂ distribution in the Baltic Sea [34].

Till now, nearly all the pCO₂ related studies in the Baltic Sea were based on in-situ measurements from ship and/or buoys, and the findings are often valid for limited sites of the sea. Therefore, analyzing variables’ relevance and obtaining reliable pCO₂ maps is critical for better understanding the carbon cycle and the air-sea exchange in the Baltic Sea [35].

3. Data

We chose the variables for pCO₂ estimation based on previous studies and the characteristic of the Baltic Sea. The variables SST, photosynthetically available radiation (PAR), Chl-a, Kd₄₉₀ nm, and a_{CDOM} were remotely sensed. SSS and MLD were produced by the numerical model NEMO-NORDIC together with data assimilation. In-situ pCO₂ measurements from three different sources were used to train and validate the model for pCO₂ estimation.

3.1. Remote Sensing Products

The Moderate Resolution Imaging Spectroradiometer (MODIS) on board Aqua satellite was designed for ocean surface investigations. The sensor maps the earth every two days from July 2002 on. A MODIS image consists of 36 spectral bands covering the spectrum of wavelength from 0.63 to 14.38 µm. Images from MODIS Aqua have been successfully used to detect coastal water clarity [36], survey red tides [37], map lake suspended matter [38], and retrieve coastal dissolved organic carbon [39]. Variables, like Chl-a and SST retrieved from MODIS-Aqua images with already mature algorithms, have been widely used to estimate sea surface pCO₂ or simulate sea surface CO₂ flux in different oceans and marginal seas [11,16,17,40,41]. From the National Aeronautics and Space Administration (NASA) Goddard Space Flight Center (<https://oceancolor.gsfc.nasa.gov/>), we obtained the level-3 monthly mean MODIS products of PAR, Kd₄₉₀ nm and SST covering the period of August 2002–October 2020. All data have a spatial resolution equivalent to 4×4 km at the equator (Table 1).

Table 1. Variables used to estimate partial pressure of carbon dioxide (pCO₂) in the study.

Data	Variables	Platform Type	Spatial Resolution	Time Span	Provider
MODIS Aqua	PAR, SST, Kd ₄₉₀ nm	Space-borne satellite	4 km	August 2002–November 2011	Ocean Color Web
MERIS	Chl-a, a _{CDOM}	Space-borne satellite	300 m	August 2002–November 2011	
NEMO-NORDIC	SSS, MLD	Model	4 km	August 2002–November 2011	CMEMS

The Medium Resolution Imaging Spectrometer (MERIS) on board Envisat satellite was designed for ocean color observation. During its life span from 2002 to 2011, MERIS mapped the earth every 1–3 days and measured water surface radiances in 15 spectral bands from visible to infrared spectrum. Up to now, MERIS data have been frequently

used to investigate water related issues in global ocean and marginal seas, including mapping sea algae coverage [42], detecting phytoplankton bloom [43] and cyanobacterial bloom [44], and estimating Chl-a, a_{CDOM} , and suspended matter [45–49]. Most of these studies targeted at European lakes and seas and demonstrated the great potential of MERIS data for investigating these waters. Specifically, [45] found that Chl-a retrieved from MERIS for the Baltic Sea had similar distributions to that of in-situ measurements.

The MERIS data from the MERCI data base (<https://merisrr-merci-ds.eo.esa.int/merci>) were used to retrieve Chl-a and a_{CDOM} for the Baltic Sea with the Free University of Berlin (FUB) processor which were especially developed for European coastal waters. Invalid pixels (i.e., land, mixture of land and water, various cloud types, and cloud shadow) were masked out from MERIS images before the Chl-a and a_{CDOM} retrieval. The performance of Chl-a and a_{CDOM} retrieved from MERIS with FUB processor in the Baltic Sea were assessed to be excellent [49,50]. In this study, the daily Chl-a and a_{CDOM} derived from MERIS images were aggregated monthly and resampled to 4×4 km. The Chl-a and a_{CDOM} derived from the full MERIS archive spans from July 2002 to December 2011. Comparison of the contributions of the Chl-a products from MODIS and MERIS to pCO_2 estimation in the method employed here did not show significant differences (Figure S2).

3.2. Modeled Data

MLD and SSS are important variables for pCO_2 estimates. However, remotely sensed SSS have much coarser resolutions than other variables, such as Chl-a, and MLD is not yet obtainable from remote sensing. Alternatively, modeled MLD and SSS have been applied in many studies on sea surface pCO_2 estimation [9,12,20,51,52]. Therefore, we employed the monthly MLD and SSS produced by the NEMO-NORDIC model which is a Baltic and North Sea model based on the NEMO ocean engine and a local singular evolutive interpolated Kalman (LSEIK) filter data assimilation with a spatial resolution of 4×4 km [53] (Table 1). Validation of the modeled SSS against the station observation demonstrated a bias smaller than 0.5 ppt and a RMSE of 0.5 ppt [53].

3.3. In-Situ Data

We used all the in-situ sea surface pCO_2 measurements available in the Baltic sea during August 2002–November 2011 (Table 2 and Figure 1). They included the data from the Surface Ocean CO_2 Atlas (SOCAT) (2nd Version) [54], the measurements from a moored buoy at Östergarnsholm site [55], and data from [56].

Table 2. The in-situ measurements used in this study.

Data Source	Acquisition Platform	Time Period	Location	No. Measurement	No. Measurements after Aggregation & Filtering
SOCAT	Ship	June 2002–October 2011	Baltic Sea	194,565	194,565
Östergarnsholm [56]	SEMI at a bouy	May 2005–December 2011	Central Baltic Sea	6631	23
	Station & ships	June 2000–September 2009	Gulf of Bothnia	6328	1060

All the data in SOCAT have undergone quality control and were of error $< 10 \mu atm$ [54,57]. We used pCO_2 measurements acquired from 2002 to 2011 to match the remotely sensed variables. The data from SOCAT for this period were obtained from the Finnpartner vessels which travelled between Lübeck and Helsinki every second day [58]. The pCO_2 measurements are available every 1–2 min and appear as a series of points distributed along the ship tracks (Figure 1A).

At the Östergarnsholm site, the sea surface pCO_2 is measured by a submersible autonomous moored instrument (SAMI) mounted on a buoy mooring one kilometer east off the island Östergarnsholm in the central Baltic Sea (Figure 1A). The SAMI sensor was installed four meters below the water surface and has recorded the pCO_2 there every 30 or 60 min from 2005 May to the present [55]. The pCO_2 measurement from Östergarnsholm site also fulfills the accuracy criterion of $< 10 \mu atm$.

The pCO₂ data used by [56] filled the data gap left by the previous two data sources in the Gulf of Bothnia. The data set consisted of both manual bottle measurements from discrete stations and continuous ferry box measurements obtained with the same method as the vessel data in SOCAT (Figure 1A). The measurements were mainly from the year of 2006, 2009, and 2010. More details about the data are available from [56]).

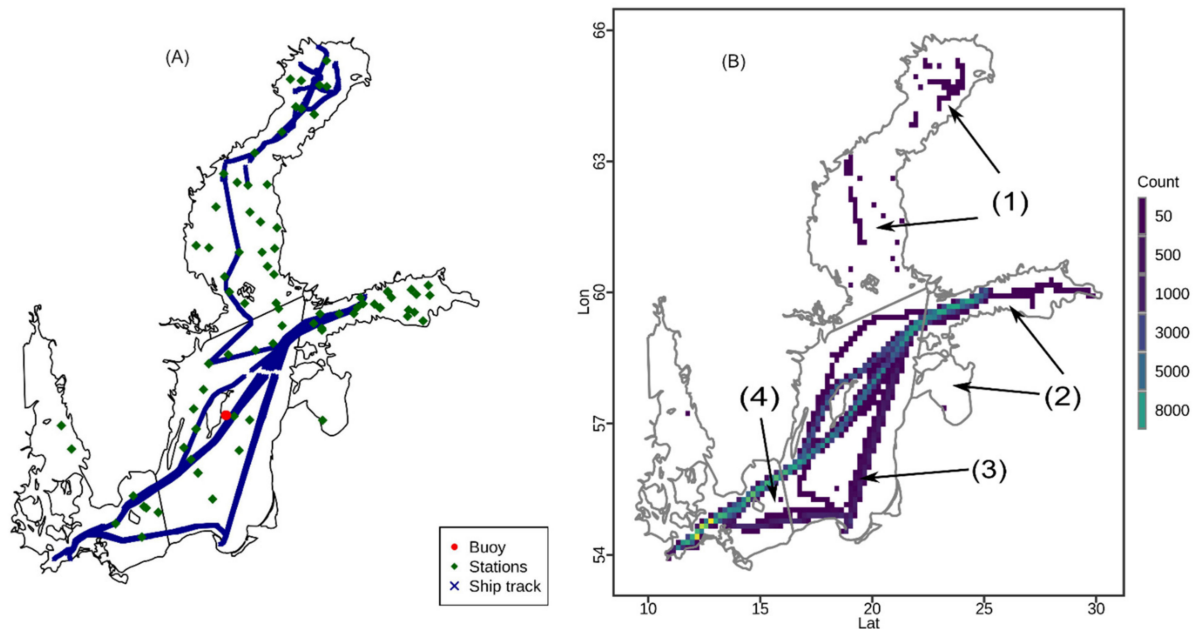


Figure 1. The location where the in-situ pCO₂ were measured in the Baltic Sea from August 2002 to November 2011 (A) and the density distribution of the in-situ pCO₂ measurements (B). The numbers in parentheses indicate the sub-basins where the variables' importance was analyzed. (1) Gulf of Bothnia, including Bothnia Bay (north) and Bothnia Sea (south); (2) Gulf of Finland (north) and Gulf of Riga (south); (3) Baltic Proper; (4) Arkona Basin.

4. Methods

4.1. Random Forest

Random forest is a tree-assembled model where the trees are constructed based on a set training samples [59]. Random forest has shown excellent performance in classification and regression [60,61]. Therefore, it has been used in various fields. For example, it has been used to estimate gross primary production of vegetation from remote sensing images [62], downscaling the soil moisture data and chlorophyll fluorescence of coarse resolutions etc. [63,64]. With respect to pCO₂ estimation from remote sensing data [17] derived pCO₂ maps for the Gulf of Mexico with an RMSE of 31.7 μ atm using a similar tree-based algorithm. In addition, [16] compared random forest with other commonly used approaches (e.g., multiple linear regression) and proved that random forest was a robust algorithm for sea surface pCO₂ estimation from remote sensing data in the Gulf of Mexico [16].

In this study, random forest models were trained to express the relationship between the in-situ pCO₂ measurements and spatially and temporally co-located variables (i.e., Chl-a, a_{CDOM}, SST, PAR, K_{d490nm}, SSS, and MLD). Each random forest model contained a number of tree (known as Ntree) with each node splitting to a number of leaves (known as Mtry). At each node, a bootstrapped subset of randomly selected training samples was used to construct the relationship between the Mtry variables (e.g., Chl- and SST) and the dependent variable (i.e., pCO₂) in the form of split leaves [65]. The tree grew as the nodes were produced and connected in a cascade manner. Each decision tree was independently produced. The forest construction was finished as the trees grew to Ntree, a user-defined number of trees [59]. The final random forest is a set of trees with best

performance in expressing the relationship between variables in the training samples. Further details on the random forest model are to be found in Breiman (2001). Each random forest model contained 500 trees ($N_{tree} = 500$) of the leaf size of three ($Mtry = 3$). We used the random forest algorithm implemented in the package randomForest [66] for the open access software R [67].

Subsequently, the importance of each variable in the random forest model was also extracted and analyzed. The importance of a variable X_m was determined by the mean decrease accuracy (MDA) of the random forest model when the variable X_m is randomly permuted in the training samples [59]. Therefore, the importance of variable X_m in a random forest model indicates its contributions/relevance to the model and the response of corresponding variable to the pCO_2 variation in the training data set. For each variable, the importance was derived independently. The variables are not complementary to each other in pCO_2 estimate. Therefore, the sum of the variables' importance cannot stay as constant value, like 100%, across different time and spatial scale.

4.2. Filtering In-Situ Data

The diurnal differences of sea surface pCO_2 in the Baltic Sea can reach up to 40 μatm [68], and using only the data from day time or night time would introduce 8% to 36% error on monthly air–sea CO_2 fluxes [69]. Pre-analysis also found that using in-situ pCO_2 measurements from 24 h for sea surface pCO_2 estimation would increase the uncertainty of results by 30–60 μatm (Supplementary Materials Figure S2). Therefore, we only used the in-situ pCO_2 measurements obtained during the exact period of the two satellites (i.e., MODIS Aqua and MERIS) passes over the Baltic Sea, i.e., 9:00–14:00 UTC 00. Subsequently, the in-situ data were aggregated monthly to match the frequency of the remotely sensed and modelled variables. The variables exactly co-located to the in-situ pCO_2 measurements were extracted and used for random forest model construction and validation.

Using the variables (e.g., SST) derived for the months characterized with frequent upwelling occurrences can significantly affect the monthly pCO_2 estimates by introducing large biases (Figure S3). Therefore, the upwelling effect should be eliminated to the largest possible extent. To achieve this, we constructed a random forest model using in-situ data from each month as validation data and the rest as training data. All the models with the alternative absence of in-situ data from each month were constructed with identical settings. Inspection on the mean absolute errors (MAE) and RMSE of these models showed that the following monthly data were dominated by upwelling (i.e., large bias): 2003–09, 2006–09, 2006–08, 2009–07, 2009–09, 2009–10, 2011–04, 2011–08, 2011–09, 2011–10 (Figure S4). Nearly all of them were in fall when upwelling prevails in the Baltic Sea [32]. In-situ pCO_2 measurements from these months were eliminated from training and validating the model. Sea surface pCO_2 maps in these months were not predicted as it would produce misestimation for these months.

After narrowing the time window of in-situ pCO_2 measurements down to 9:00–14:00, aggregating these in-situ pCO_2 measurements monthly, and filtering out the data from the upwelling dominated months, 10,769 in-situ pCO_2 measurements with matching variables remained, as shown in Figure S1.

4.3. Analyzing Variables' Importance for pCO_2 Estimation

We derived the variables' importance to the pCO_2 estimation on two scales: spatially and temporally. On the spatial scale, the random forest models were constructed both for the overall Baltic Sea and its sub-basins indicated in Figure 1B. In each sub-basin, a random forest model was trained with the in-situ in the sub-basin from 2/3 of the months from random selection. Each model was then validated with the in-situ data in the sub-basin from the rest 1/3 months. We constructed 50 random forest models in each sub-basin with the training and validation data selected in such way. In the temporal analysis of the variables' importance to the pCO_2 estimates, the in-situ measurements were divided

into different seasons. Specifically, February–April was spring, May–July was summer, and August–October was fall. The limited availability of satellite data due to frequent and extensive cloud coverage in November, December, and January did not allow for such analysis during these months. Like the spatial analysis, in-situ data from 2/3 of the months from random selection were used for training and the rest 1/3 for validation. Fifty random forest models were constructed in each season with the training data selected in the same manner and validated with the corresponding complementary data.

4.4. Constructing the Final Model for pCO₂ Estimation in the Baltic Sea

We constructed a final random forest model for pCO₂ estimation in the entire Baltic Sea. This model was trained with the in-situ pCO₂ measurements in odd months of even years (e.g., March 2002) and even months of odd years (e.g., April 2003) and validated with the remaining data. By doing this, both the training and validation data covered each of the 12 months in a year and the pCO₂ relevant processes from each month. Exchanging the training data and validation data yielded models with nearly the same performance (Figure S7). The monthly mean pCO₂ distribution in the entire Baltic Sea were predicted with this model.

The Pearson correlations of the pCO₂ estimated with above model to each of the variables were analyzed. In order to speed up the processing, the correlation was analyzed on a 0.5° × 0.5° grid form. In each month, the mean of pCO₂ and the means of each targeted variables (e.g., Chl-a) in the same grid cell was derived. The Pearson correlations between pCO₂ and each of the variables in each grid cell were obtained across the study period of 2002–2011.

4.5. Comparing the Random Forest to Self-Organized Map (SOM) and Multiple Linear Regression (MLR) for pCO₂ Estimation in the Baltic Sea

SOM is an artificial neuronal network algorithm which classifies the input samples into a number of classes, based on their Euclidian distance from each other in the space determined by the variables of the input data [20,70]. Often, the number of classes (neuron) are given a priori in a grid format (e.g., 2 × 5). Each class corresponds to a neuron which contains the coefficients determining the relationship between the variables and the dependent variable in the same class, which is also called labelling the class with the dependent variable (output). In the case of sea surface pCO₂ estimation with SOM, the remotely sensed variables, like Chl-a and SST, in the training data, are used to calculate the distance between the input samples for classification. In the pCO₂ prediction with such a SOM model, the samples will be attributed with the pCO₂ of a class to whom the sample show the closest distance to. Detailed description of a SOM application for sea surface pCO₂ estimation by remote sensing data is available in Telszewski et al. (2009). SOM and its variants have been widely used to estimate sea surface pCO₂ with support of remote sensing products [11,12,20,71–74]. In this study, we used the SOM algorithm implemented in the R packages of kohonen [75]. We set the size neurons (class) grid to be 25 × 20, in order to have the total number of classes same to the number of trees in the random forest models constructed in this study.

Furthermore, multiple linear regression (MLR) has been used in many studies for estimating sea surface pCO₂ in marginal seas and performed good results [9,16]. Therefore, we compared the performance of SOM, MLR, and random forest in the sea surface pCO₂ estimation in the Baltic Sea. During the comparison, the same variables were used in the three algorithms without any preselection. Random forest, SOM, and MLR models were trained with the identical data and validated likewise.

Two schemes of training data selection were adopted, one with in-situ pCO₂ measurements from 2/3 of the months from random selection (scheme Number 1, same as in Section 4.3) and the other one using 2/3 of in-situ pCO₂ measurements from random selection as training data (scheme Number 2). Scheme Number 2 was similar to the training data selection by [12]. In both schemes, the validation data were the complementary of the training data.

5. Results

5.1. Spatiotemporal Characteristics of Variable Importance to pCO₂ Estimation

On the entire Baltic Sea scale, PAR was the most important variable (mean importance of 66%) for the sea surface pCO₂ estimate during 2002–2011. It meant that the errors of the random forest model constructed without PAR would be by 66% higher than that constructed with PAR. PAR was followed by SST, MLD, a_{CDOM}, and SSS with mean importance of 21%, 20%, 15%, and 14%, respectively. Chl-a and Kd_{490nm} showed the lowest importance of 12% and 10% (Figure 2A).

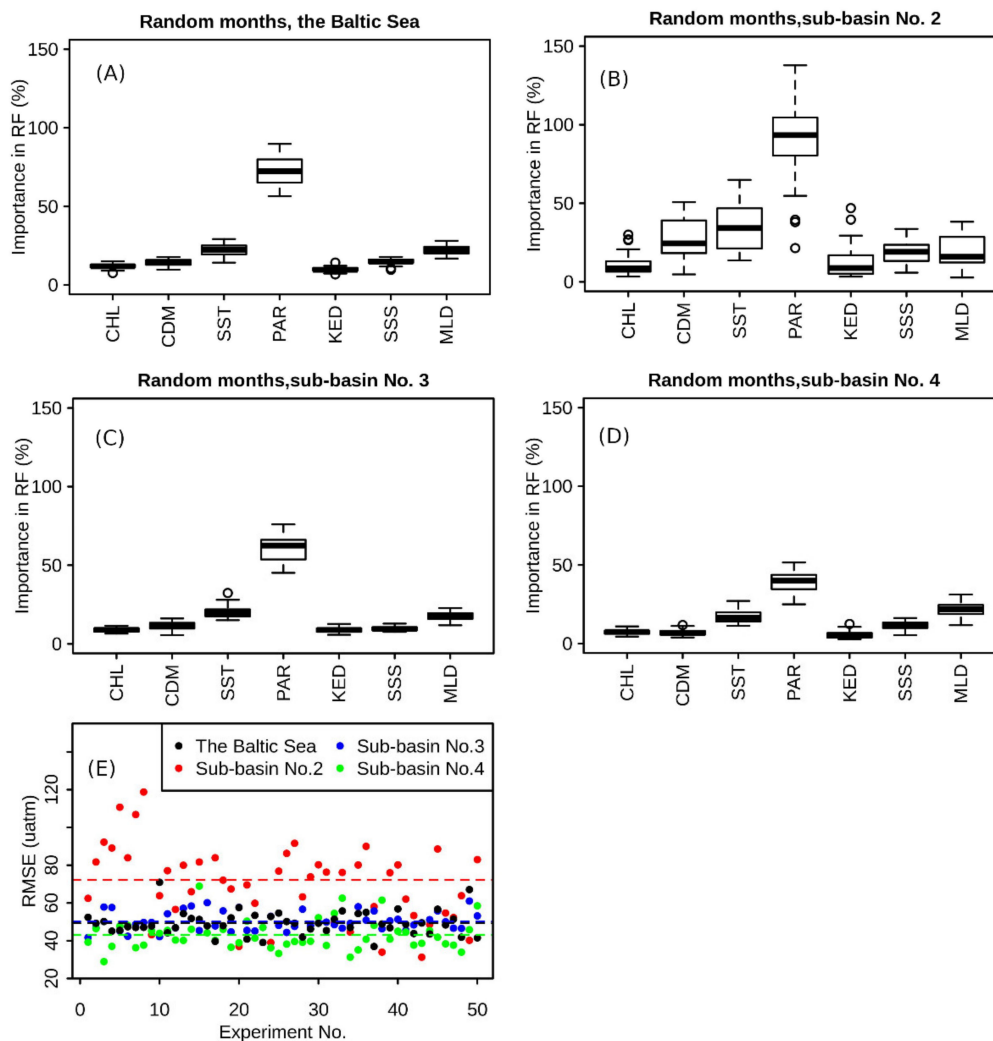


Figure 2. Variables' importance for pCO₂ estimate in the Baltic Sea and its sub-basins. (A) Variables' importance in the 50 models trained with in-situ data in the entire Baltic Sea from 2/3 months of random selection; (B–D) Variables' importance in the 50 models trained with in-situ data from each sub-basin from 2/3 months of random selection. (E) The RMSEs of the 50 models trained with in-situ data from the four regions, respectively. CDM in the sub-figures donates the a_{CDOM} derived from Medium Resolution Imaging Spectrometer (MERIS) images, KED stands for Kd_{490nm}.

The variables importance differed among the sub-basins of the Baltic Sea. Compare to the pCO₂ estimate in the entire Baltic Sea (Figure 2A), the importance of PAR, SST, a_{CDOM}, SSS, and MLD for pCO₂ estimation in the Gulf of Finland (i.e., sub-basin No.2) increased by 26%, 13%, 15%, 5%, and 1% (Figure 2B). For pCO₂ estimation in this sub-basin, PAR was still the most importance variable. With the mean importance of 25%, a_{CDOM} and SST are the next most importance variables, followed by SSS and MLD with respective importance of 18% and 16% (Figure 2B). The importance of Chl-a and a_{CDOM} to the pCO₂ estimation in

the southern Baltic Sea (i.e., sub-basins No.3–4) were similar to that for the overall Baltic Sea, with slightly lower importance of SSS in sub-basin No.3 (Figure 2A). The filtering and time window narrowing down left the Gulf of Bothnia (i.e., sub-basin No.1, Figure 1) with the in-situ data from March 2006 and September 2009. It hampered the construction of random forest model for pCO₂ estimate in this sub-basin, due to the strategy of data from 2/3 months for model training. The 50 random forest models constructed in the Baltic Sea, sub-basin No.2, sub-basin No.3, and sub-basin No.4 had the means of 49 μatm , 72 μatm , 50 μatm , and 43 μatm , respectively.

The variables' importance for pCO₂ estimation also varied on seasonal scales. For the sea surface pCO₂ estimate in the entire Baltic Sea during February–April, PAR was the most important variable with mean importance of 56%, followed by MLD (20%), SSS (15%), SST (15%), and a_{CDOM} (10%). Chl-a and Kd_{490nm} showed mean importance of 8% (Figure 3B). From May to July, all the variables displayed a similar importance (12–14%), with Kd_{490nm} (7%) and MLD (5%) (Figure 3C). The low importance of all the variables in May–July means that during this period the alternative absence of the variables in the models constructed did not significantly change the accuracies of the respective models. In another word, during May–July, the combination of any six out of the seven variables used in the study can well cover the variations of pCO₂ in the Baltic Sea. For pCO₂ estimation in the entire Baltic Sea in the period of August–October, PAR and SST were the first two most important variables with respective importance of 38% and 31% (Figure 3D), followed by MLD (16%) and SSS (12%) and the rest variables with importance of 10%. Chl-a and Kd_{490nm} showed overall low importance for the pCO₂ estimate across Baltic Sea, regardless of the season. From November to the following January, the dense cloud cover over the Baltic Sea region barely allowed any optical images qualified for the retrieval of remote sensed variables. The RMSEs of the 50 models were in the range of 30–80 μatm . The models trained with data from May–July showed the smaller RMSEs (41 μatm) than those trained with in-situ data from February–April and August–October (52 μatm and 55 μatm) (Figure 3D).

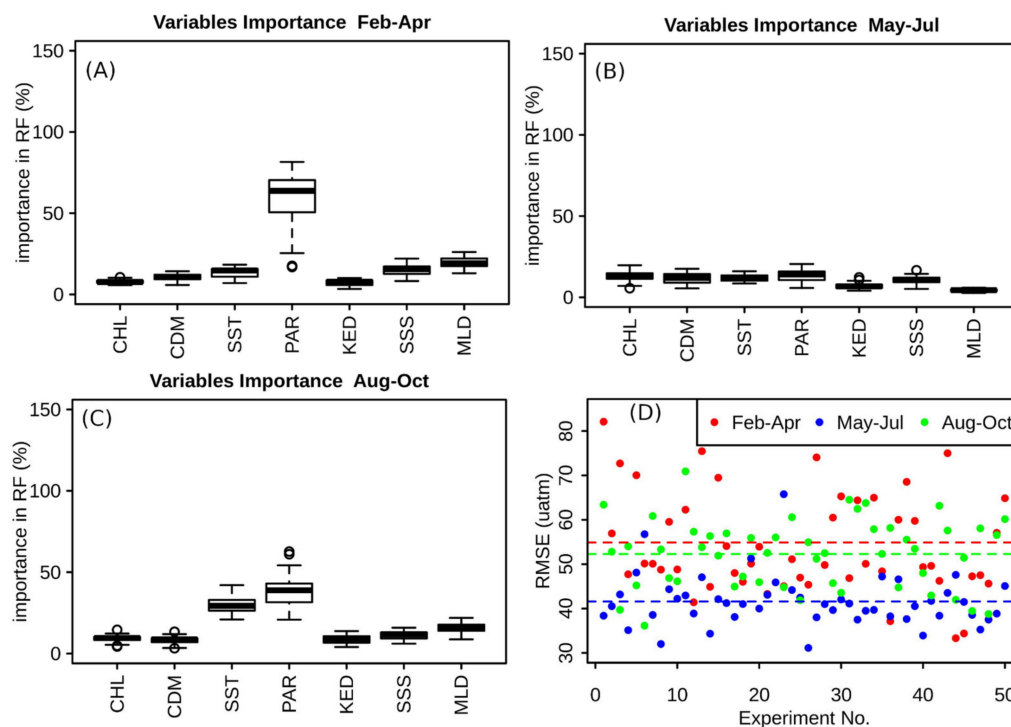


Figure 3. Variables' importance for pCO₂ estimate in the entire Baltic Sea in different seasons (A–C) and the RMSEs of the corresponding 50 models (D).

Overall, PAR showed the highest importance for pCO₂ estimate in the Baltic Sea across different seasons and locations. SST was the second most important variable. a_{CDOM} is important for pCO₂ estimate in the Gulf of Finland. MLD is important for pCO₂ estimate in all the sub-basins of the Baltic Sea but varied seasonally. SSS is important for pCO₂ estimation in the Baltic Sea both spatially and temporally. Chl-a, which has been commonly considered as the determining variable for pCO₂, showed low importance to the pCO₂ estimate over the entire Baltic Sea and its sub-basins. Kd_{490nm} showed low importance for pCO₂ estimation in the Baltic Sea across different seasons and sub-basins.

5.2. pCO₂ Maps from Final Random Forest Model

The final random forest model for sea surface pCO₂ estimation for the entire Baltic Sea engaged all the variables, namely, PAR, Chl-a, a_{CDOM}, SST, Kd_{490nm}, SSS, and MLD. Its RMSE was 47.8 µatm and its coefficient of determination (i.e., R²) was 0.63 (Figure 4A). The mean absolute error (MAE) of the model was -3.26 µatm, implying a slight overall underestimate of pCO₂. The pCO₂ predicted with this model exhibited minor overestimates for pCO₂ larger than 450 µatm and slight overestimates for pCO₂ around 200 µatm (Figure 4A). Both the estimated and observed pCO₂ values were mainly in the range of 100–500 µatm, with a few pCO₂ observations between 500 µatm and 600 µatm (Figure 4A).

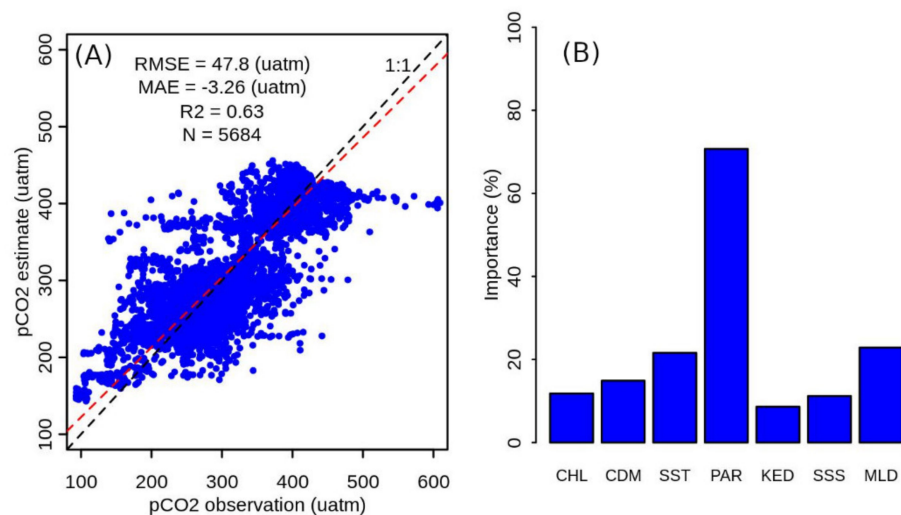


Figure 4. The final random forest model for the pCO₂ estimate. (A) Quality performance of the model, where the red dashed line is the regression line between the pCO₂ observation and the estimate and black dashed line is 1:1 line; (B) the variables' importance in the model.

The variable importance in the final model was similar to that in Figure 2A. Specifically, PAR was the most important variable, followed by SST, MLD, and a_{CDOM}. Ch-a and Kd_{490nm} showed the lowest importance (Figure 4B).

For the period of August 2002–October 2011, pCO₂ maps covering the entire Baltic Sea were retrieved for each month except November, December, January, and February, when the remotely sensed variables were not available due to frequent cloud coverage. Taking the year of 2005 as example (Figure 5), the sea surface pCO₂ in the Baltic Sea were in the range of 100–500 µatm. On the spatial scale, the pCO₂ maps exhibited reasonable transitions in the Baltic Sea (Figure 5). In addition, detailed features of the pCO₂ variation were also displayed in those maps. For example, in April 2005, much lower pCO₂ was present at the river mouths in the southern Baltic Sea compared to other areas. In May 2005, a strip of low pCO₂ was present in the central Baltic Proper. In September 2005, an area of pCO₂ higher than both August and October was displayed in the southern Baltic Sea (Figure 5).

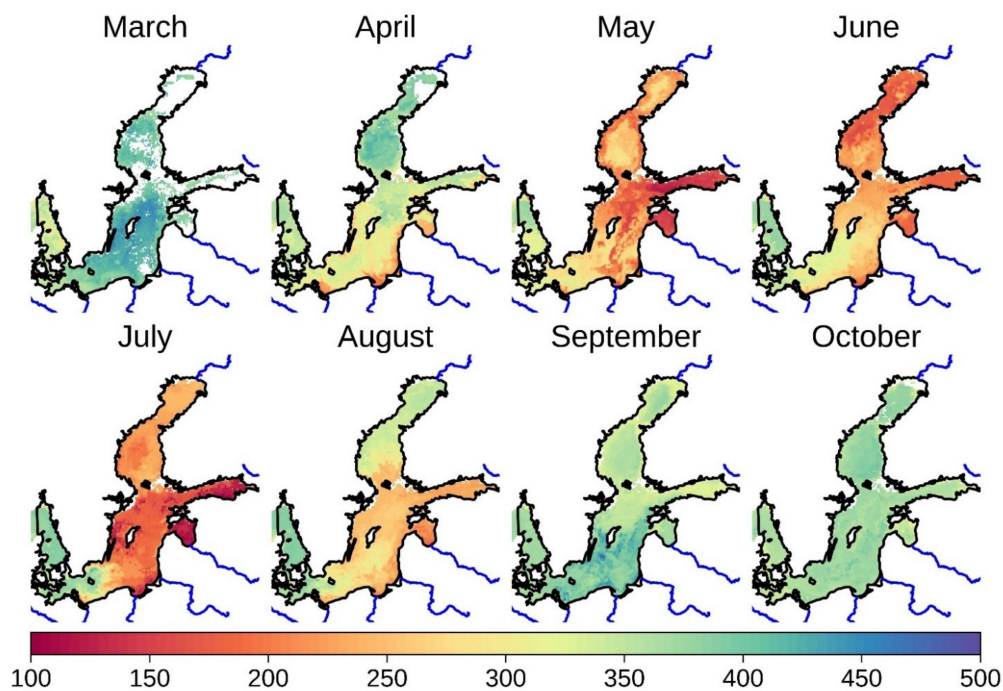


Figure 5. Seasonal distribution of $p\text{CO}_2$ in the Baltic Sea in the year of 2005 and the large rivers draining to the Baltic Sea.

The sea surface $p\text{CO}_2$ in the Baltic Sea exhibited significant seasonal variations (Figure 5). Generally, low (undersaturated) $p\text{CO}_2$ conditions of 100–300 μatm prevailed during summer months (e.g., July) and the winter months (e.g., October) were characterized by oversaturated $p\text{CO}_2$ conditions of up to 500 μatm (Figure 5). The $p\text{CO}_2$ variation at different sites in the Baltic Sea also exhibited these characteristics (Figure 6).

The sea surface $p\text{CO}_2$ in the Baltic Sea also showed significant spatial gradient and variation along the months, particularly between April and September (Figure 5). In April, July, and August, the southern central Baltic Sea (excluding the sub-basin No.4 in Figure 1B) often displayed $p\text{CO}_2$ approximately 100–150 μatm lower than the northern sub-basins (Figure 5). In May, the Gulf of Finland and the Gulf of Riga (Sub-basin No.2 in Figure 1B) showed the lowest $p\text{CO}_2$ of 100 μatm in the Baltic Sea. In June, sea surface $p\text{CO}_2$ in the two narrow gulfs increased slightly, while the Gulf of Bothnia exhibits its lowest sea surface $p\text{CO}_2$ in a year. In September, the sea surface $p\text{CO}_2$ in the southern Baltic Sea increased rapidly and displayed a reversed the gradient to that in August. In October, the $p\text{CO}_2$ in the entire Baltic Sea was in the range of 380–420 μatm , rather homogenous in comparison to other months (Figures 5 and 6). On the other hand, different areas in the Baltic Sea showed their minimum $p\text{CO}_2$ at different time. While the Gulf of Finland (No.42 in Figure 6A) and the Baltic Proper (i.e., No.61 in Figure 6A) had two seasonal minima in May and July, respectively, the Bothnia Sea (i.e., No.8 in Figure 6A) and the Bothnia Bay (No.28 in Figure 6A) showed their only seasonal minima of 180–250 μatm in June. Thirdly, the seasonal change points of $p\text{CO}_2$ into the Baltic Sea varied spatially. The $p\text{CO}_2$ in the Bothnia Bay and Bothnia Sea started decreasing in May (Figure 6B,C), but the $p\text{CO}_2$ in the Baltic Proper and Gulf of Finland in the south showed this change already in April, one month earlier (Figure 6D,E). The $p\text{CO}_2$ in the Gulf of Bothnia (i.e., No.8 and 28 in Figure 6A) increased already in July, but such changes in the $p\text{CO}_2$ in the southern Baltic Sea were delayed by one month to August. Consequently, in August, when $p\text{CO}_2$ in the northern Baltic displayed are almost equal to the values in winter months (Figure 6B,C), $p\text{CO}_2$ in the Baltic Proper and Gulf of Finland remained on the level of its summer value (Figure 6D,E). Furthermore, in the Gulf of Finland (i.e., No.42 in Figure 6A), significant inter-annual $p\text{CO}_2$ differences were present in April and August (Figure 6D), but, in the Baltic Proper (i.e., No.62, Figure 6A), this occurred in May, July, and August (Figure 6E).

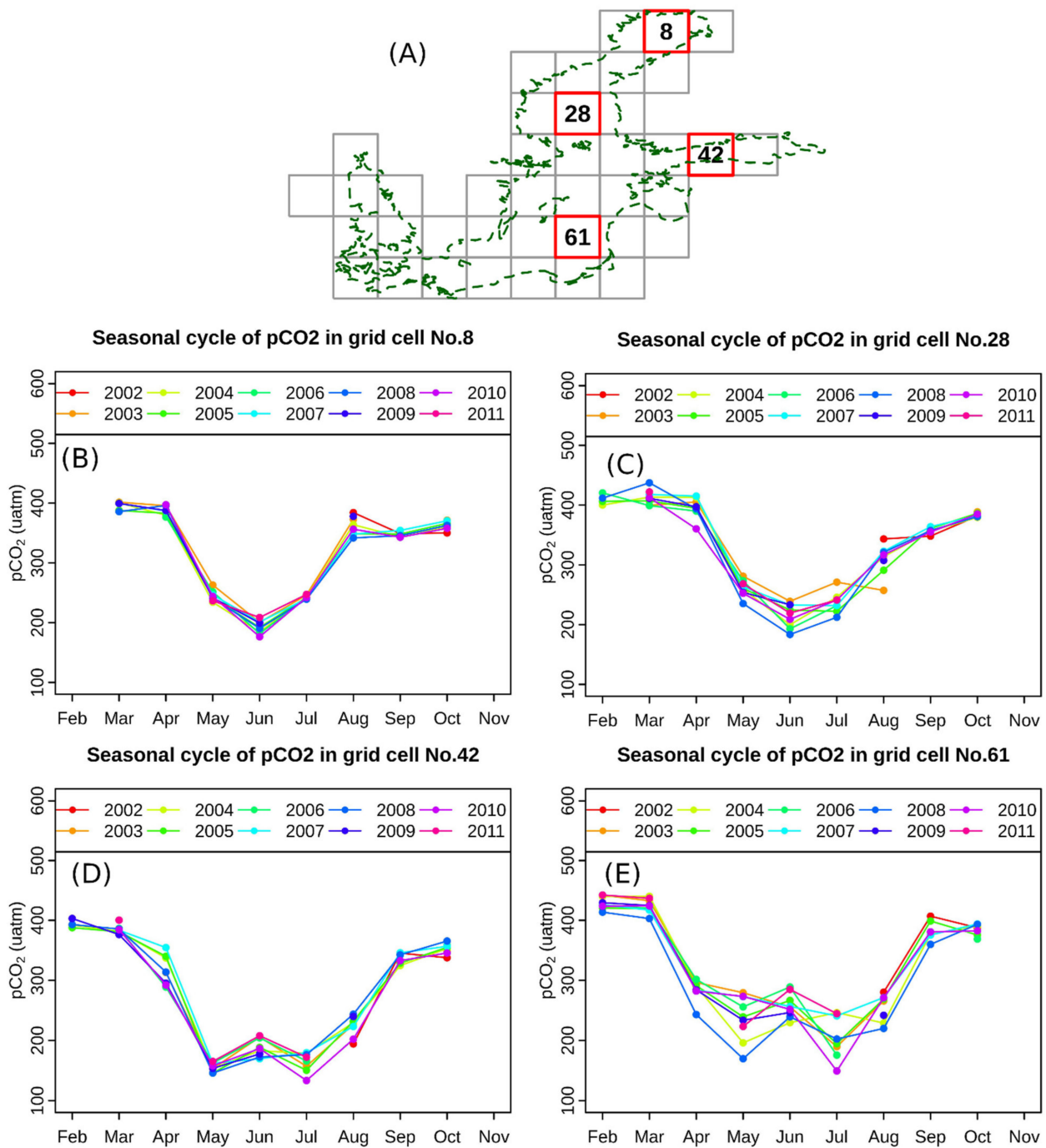


Figure 6. Seasonal cycle of monthly pCO₂ at different sites in the Baltic Sea. The pCO₂ estimate for the months determined with significant upwelling effect in Section 4.2 were excluded from this analysis. (A): the location of the sites, (B–E): the seasonal cycle of monthly pCO₂ at sites in sub-figure A.

Across the period of 2002–2011, the estimated pCO₂ were correlated to the variables in the Baltic Sea to different degrees in different directions, varying spatially (Figure 7). The Chl-a-pCO₂ correlation varied between -0.5 and 0.5 , with general positive correlation in the northern Baltic Sea and negative correlation in the south. The estimated pCO₂ were generally negatively correlated to the co-located a_{CDOM} in the Baltic Sea with correlation coefficients ranging from -1 to 0 , and the correlation exhibited larger absolute coefficients than Chl-a-pCO₂ correlation, particularly in the southern Baltic Sea. SST-pCO₂ correlation mostly exhibited negative coefficients (i.e., from -0.5 to 0) in the Baltic Sea, with larger absolute values in the south than in the north. Exceptionally high positive SST-pCO₂

correlation, up to 0.8, was present in the very west part of the Baltic Sea. The PAR- $p\text{CO}_2$ correlation in the Baltic presented the largest absolute coefficients and $p\text{CO}_2$ was mostly negatively correlated to PAR in the entire Baltic Sea (i.e., from -1 to -0.6), showing the same pattern to the SST- $p\text{CO}_2$ correlation. $\text{Kd}_{490\text{nm}}$ - $p\text{CO}_2$ correlation showed the similar pattern as Chl- a - $p\text{CO}_2$, with slightly higher absolute coefficients in the southeastern coasts. SSS exhibited high positive correlation to the co-located $p\text{CO}_2$ at the coastal waters with values ranging from 0 to 0.8, mostly at 0. MLD was positively correlated to $p\text{CO}_2$ in the entire Baltic Sea with large absolute coefficients (0.5–1), except in the very north and west part of the sea.

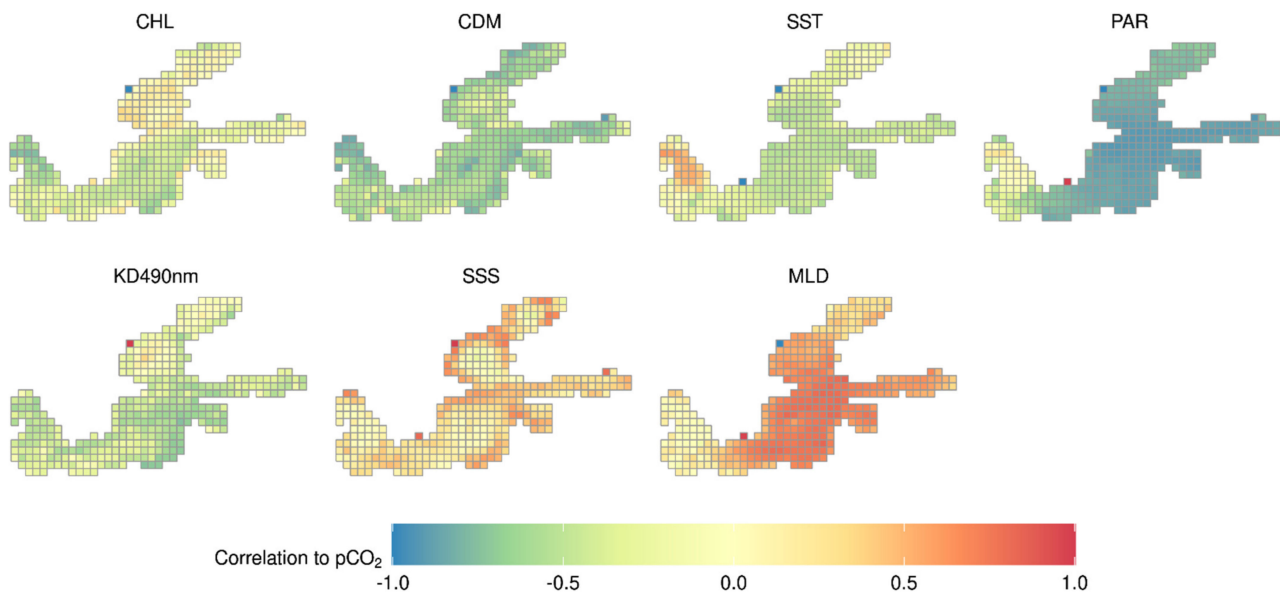


Figure 7. The spatial correlation between the estimate $p\text{CO}_2$ and the variables the study period of 2002–2011. The size of grid cells is $0.5^\circ \times 0.5^\circ$. Minus value the variable was negatively correlated to the $p\text{CO}_2$ there and the positive values mean positive correlations.

5.3. Comparison of Random Forest and SOM

In the both schemes of training and validation data selection described in Section 4.5, majority of validation data were in the range of 100–500 μatm . The $p\text{CO}_2$ estimated with random forest were in the same range as the validation data (Figure 8A,C). In contrast, the SOM model constrained the $p\text{CO}_2$ estimate into the range of 230–430 μatm (Figure 8A,C), particularly in the scheme No.2 where the training data were the randomly selected $p\text{CO}_2$ measurements (Figure 8C). In addition, often one $p\text{CO}_2$ value estimated from SOM responded to a large range of observed $p\text{CO}_2$, forming evident horizontal features in the cross-validation (Figure 8A,D), particularly when the prediction covers multiple months. However, such patterns were not notable in the $p\text{CO}_2$ estimated with random forest or MLR (Figure 8B,E).

In an example of 50 experiments where the training data were selected with scheme No.1 (Figure 8A,B), the coefficient of determination of the random forest model prediction was 0.68, much larger than 0.58 and 0.6, the coefficient of determination of the prediction with the SOM and MLR trained with the identical $p\text{CO}_2$ measurements. The mean RMSE of the 50 random forest models trained with training data selected with scheme No.1 was 49 μatm , while the mean RMSE of their SOM and MLR counterparts were 55 and 62 μatm (Figure 8C). In the case of training data selected with scheme No.2, the mean RMSE of the 50 random forest models was 24 μatm , significantly lower than 30 and 48 μatm , the respective means of RMSEs of the 50 SOM models and MLR models trained with the same sets of training data (Figure 8F). This indicated random forest outperformed SOM in the $p\text{CO}_2$ estimation in the Baltic Sea.

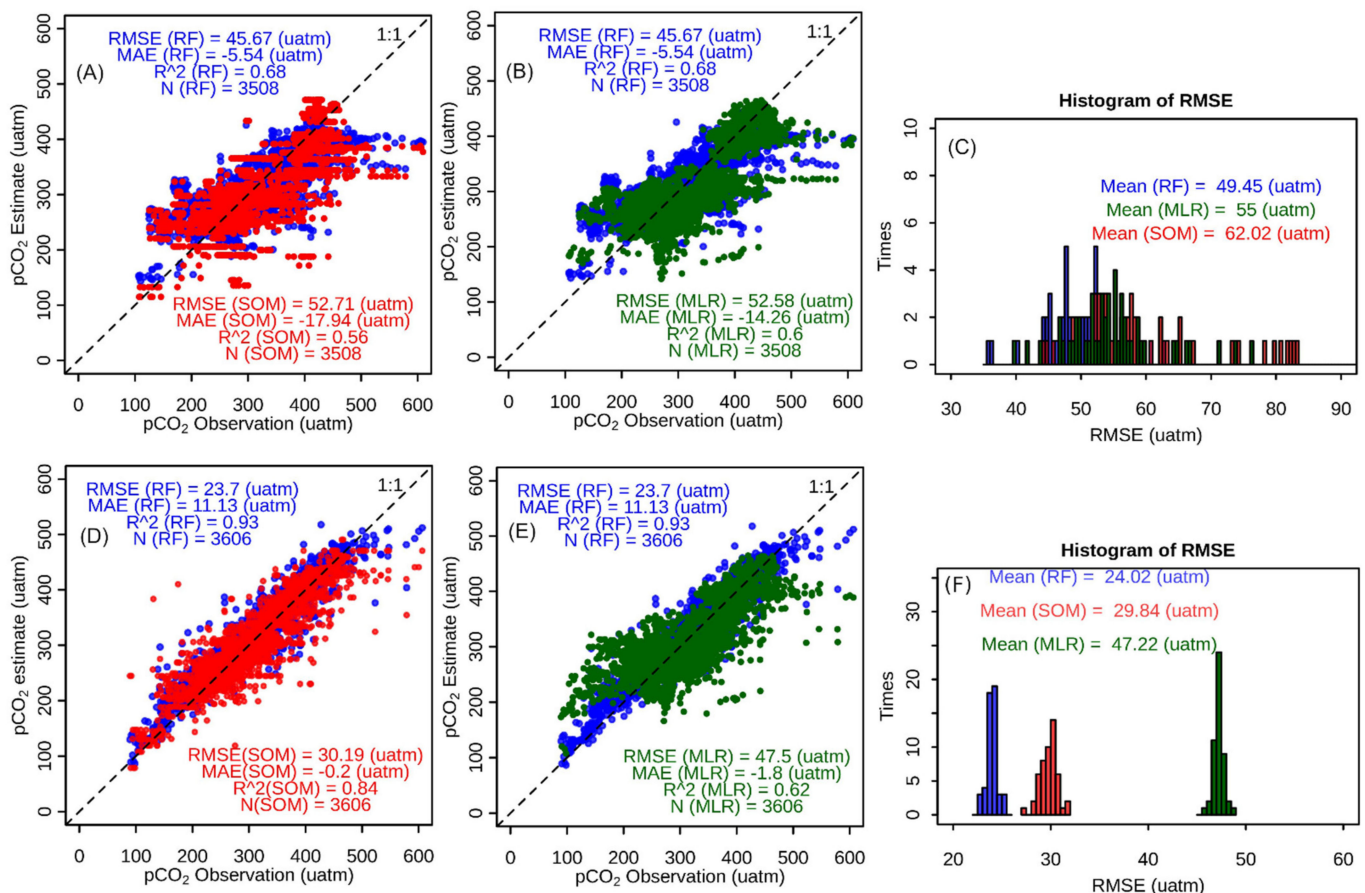


Figure 8. Comparison of random forest, SOM, and multiple linear regression (MLR) in pCO₂ estimation in the Baltic Sea. (A,B) Comparison of a random forest model (i.e., RF in the figures) to the SOM model and MLR model trained with exactly the same in-situ data from 2/3 of months selected randomly; (C) Histograms of RMSE of 50 models trained in the same manner as in A and B; (D,E) Comparison of a random forest model to the SOM model and MLR model trained with exactly the same 2/3 of the in-situ data selected randomly; (F) Histograms of RMSE of 50 models constructed the same manner as in (D,E).

6. Discussion

6.1. Characteristics of Variable Contribution to the pCO₂ Estimate

We analyzed the importance of different variables to the pCO₂ estimation in the Baltic Sea using random forest on different spatial and temporal scales. It was evident that the spatiotemporal variability in the variable's importance was high, but some general patterns were visible.

Chl-a displayed overall low importance (small contribution) to the pCO₂ estimate across different spatial and temporal scales in the Baltic Sea (Figures 2 and 3). The Chl-a-pCO₂ correlation in the Baltic Sea was also relatively low, compared to the other variables' correlation to pCO₂ (Figure 7). This was in contrast to previous findings that Chl-a was closely related to pCO₂ in global oceans [13] and marginal seas, like the Gulf of Mexico [10]. The limited importance of Chl-a is probably due to: (1) In addition to Chl-a, PAR, and SST are also fundamental factors for the photosynthesis induced biological fixation of carbon; (2) The studies that established or confirmed correlations between Chl-a and pCO₂ did not include a_{CDOM} [13,76]. But high correlation ($r > 0.9$) was found between remotely sensed Chl-a and a_{CDOM} in the Gulf of Mexico [17] and West Florida Shelf [41]. Chl-a and a_{CDOM} also displayed similar spatiotemporal patterns in the Baltic Sea (Figure S8). In the analysis of variables' importance, a_{CDOM} exhibited a more pronounced response to pCO₂ variation than Chl-a (Figure 2A), as it showed higher correlation to pCO₂ than Chl-a did (Figure 7).

Similarly, sea surface $p\text{CO}_2$ in the Gulf of Mexico is more closely related to a_{CDOM} than to Chl-a [41]. However, despite its low importance for sea surface $p\text{CO}_2$ estimate in the Baltic Sea at all the spatial and temporal scales and its general low correlation to $p\text{CO}_2$ (Figures 2, 3 and 7), we still regarded Chl-a as an important variable for the $p\text{CO}_2$ estimation in the Baltic Sea. This is particularly the case during summer (i.e., May–July), when the cyanobacteria and phytoplankton blooms takes place often, uptakes CO_2 and reduces the sea surface $p\text{CO}_2$ in the Baltic Sea [58]. The low importance of Chl-a in May–Jul (summer in this study) (Figure 3B) is very likely that, during this time, the effect of absent Chl-a in the model was compensated by variables highly correlated to Chl-a during in this time (e.g., CDOM and SST). Likewise, the other variables also exhibited low importance for $p\text{CO}_2$ estimate in May–July (Figure 3B). Yet, this was the case for the Baltic Sea, as for its applicability in other marginal seas, and the situation should be treated carefully.

Overall, PAR exhibited the highest importance for the $p\text{CO}_2$ estimation in the Baltic Sea across different sub-basin and nearly in every season, except summer. In addition, the PAR- $p\text{CO}_2$ correlation coefficients were of the largest absolute values among all the variable- $p\text{CO}_2$ correlations (Figure 7). The high importance of PAR for $p\text{CO}_2$ in the Baltic Sea and its sub-basins and the high correlation of this variable to sea surface $p\text{CO}_2$ are attributed to the high seasonality of the sun illumination. Located at the high latitude of the Baltic Sea $54\text{--}66^\circ\text{N}$ (Figure 1), the sun illumination in the central Baltic Sea, for example, varies from 6 h in winter to 18 h in summer. As phytoplankton photosynthesis is largely determined by the available sun illumination, it is reasonable that seasonality of $p\text{CO}_2$ aligns with that of PAR. In addition, river discharge loaded with CDOM, etc. is also characterized with high seasonality and, to large extent, synchronized to PAR [30], so is the bacteria respiration dependent on the available organic matter. Therefore, it is reasonable that PAR exhibited high importance for sea surface $p\text{CO}_2$ estimation in the Baltic Sea and its sub-basins. The importance of PAR in the $p\text{CO}_2$ estimate in the Baltic Sea in different seasons can be attributed to the wide span of the Baltic Sea (12°) in latitude (Figure 1) and the resultant large gradient in sun illumination. On a day in spring, the sun illumination in the southern Baltic Sea is 2–3 h longer than that in the north, same for fall. The gradients in PAR largely impose differences in the intensities of phytoplankton photosynthesis, SST distribution, and ultimately to CO_2 uptake of sea water via primary production. As for in summer when PAR and other variables displayed similar but low importance, sun illumination in the northern Baltic Sea is up to 6 h longer than in the southern Baltic Sea, displaying an even larger spatial gradient across the Baltic Sea than in other seasons. However, owing to snowmelt, the co-current freshwater discharge and the nutrients it loads are all very high in the Baltic Sea in late spring and early summer [30], create a high spatiality in the nutrient and DOM etc. Yet, the spatial pattern of cDOM etc. are likely different from that of PAR, depending on the sizes of catchment and land cover types. When all the processes determining $p\text{CO}_2$ take place with similarly high intensities, none of the variables exhibit prominent importance, but all of them jointly determined the $p\text{CO}_2$ in the Baltic Sea in summertime with similar degree (importance).

Concerning the determination of the seasonality in sea surface $p\text{CO}_2$, the Julian day of the year (DOY) has been frequently in previous studies [12,16]. However, in this study, PAR holds two advantages over DOY. Firstly, PAR is a direct measure of sun radiation available for photosynthesis, and it has physical meaning, while DOY is a proxy of the seasonality. Secondly, a trigonometric conversion is often applied on DOY to correctly proximate the seasonality. Specifically, the minus cosine of DOY was used for $p\text{CO}_2$ estimate in waters in the northern hemisphere and cosine of DOY for waters in the southern hemisphere [16,18]. Consequently, a trigonometric conversion of DOY attributes a spatially constant value in the entire hemisphere and overlook the effect spatial gradient of sun illumination. In contrast, PAR captures well the spatial gradient of sun illumination along the longitude and express its effect on photosynthesis in the water. Therefore, we suggest that future sea surface $p\text{CO}_2$ estimation consider the participation of PAR instead of DOY (Figure 1).

The SST holds the same position in the pattern of variables' importance for $p\text{CO}_2$ estimate in the Baltic Sea and its sub-basin (Figure 2). This was probably because the seasonality magnitudes of SST in each sub-basin are on the same order, particularly when the sub-basins are relatively small and well mixed horizontally. In many cases, despite its correlation to $p\text{CO}_2$ being on the same order as the Chl-a- $p\text{CO}_2$ and $K_d_{490\text{nm}}-p\text{CO}_2$ correlations, SST showed a larger importance than Chl-a, which aligned with the prediction error produced by alternatively omitting the variables by [17]. In the $p\text{CO}_2$ estimates for the Baltic Sea in different seasons, SST was more important in August–October than in other seasons (Figure 3). This was probably because, in fall, the large spatial gradient in SST in the Baltic Sea responded more to the $p\text{CO}_2$ distribution at a similar degree as the PAR does, but more than other variables. For example, the sea surface in the Gulf of Bothnia starts freezing already in October and lower down the primary production, whereas the southern Baltic Sea remains open water at time and allow the biological CO_2 uptake [77].

Despite its low importance for the $p\text{CO}_2$ estimate for the entire Baltic Sea, a_{CDOM} exhibited more important for the $p\text{CO}_2$ estimate in the Gulf of Finland than in other sub-basins (Figure 2B). The $a_{\text{CDOM}}-p\text{CO}_2$ correlation in the Baltic Sea is also relatively large, particularly at the coast and in the Gulf of Finland (Figure 7). As mentioned previously, bacteria respiration produces CO_2 by decomposing organic carbons, like DOM [14,15]. The relatively narrow waters of the Gulf of Finland receive a large terrestrial input of DOM from the rivers, including the Neva, which drains the largest sub-catchment of the Baltic Sea, approximately 1/6 of the total Baltic Sea catchment [30]. The changes of sea surface $p\text{CO}_2$ in the Gulf of Finland largely responded to the changes in CDOM there. Therefore, a_{CDOM} is important for $p\text{CO}_2$ estimation in the Gulf of Finland (Figure 2B) and thus in the Baltic Sea, as well. Similar mechanism very likely applies at coastal waters receiving river discharges. Moreover, this study used the a_{CDOM} derived from MERIS images. The MERIS sensor was succeeded by the Ocean and Land Color Instrument (OLCI) sensors on Sentinel-3 satellites in 2016. Therefore, a_{CDOM} derived from OLCI images will likely play an equivalent role in the $p\text{CO}_2$ estimate in the Baltic Sea and other similar waters.

Though less than PAR and sometimes slightly less than SST, MLD was important for the $p\text{CO}_2$ estimation in the Baltic Sea and all its sub-basins (Figure 2B). $p\text{CO}_2$ in the Baltic Sea is largely and positively correlated to MLD (Figure 7). This is probably resulted from the seasonally varying amount of fresh water discharged by the many rivers and lay above the relatively saline and heavy water [78]. In addition, seasonal winds in the Baltic Sea might have jointly determined the high variation of MLD [32] and, consequently, the vertical mixing of sea water and $p\text{CO}_2$, as well.

In this study, $K_d_{490\text{nm}}$ showed low importance to the $p\text{CO}_2$ estimation in the Baltic Sea, regardless of season or sub-basin (Figures 2 and 3) and a relatively weaker correlations to $p\text{CO}_2$ (i.e., from -0.7 to 0), compared to variables, like PAR and a_{CDOM} . This aligns with the previously found negatively correlation between $K_d_{490\text{nm}}$ and $p\text{CO}_2$ in the Gulf of Mexico [16]. Here, we argue that the reasons behind the low contribution of Chl-a to $p\text{CO}_2$ estimation very likely also applied to $K_d_{490\text{nm}}$. This argument is well supported by previous studies. It is found that $K_d_{490\text{nm}}$ in the Baltic Sea was a function of inherent optical properties, i.e., absorption and scattering of phytoplankton, and effects of illumination and viewing angle [79,80]. Furthermore, [81] observed a strong positive correlation between $K_d_{490\text{nm}}$ and river discharge into the Baltic Sea and the latter is rich of CDOM. In addition, a positive correlation of $K_d_{490\text{nm}}$ to Chl-a and a_{CDOM} were noticed in the Baltic Sea (S9), and the $K_d_{490\text{nm}}-p\text{CO}_2$ and $a_{\text{CDOM}}-p\text{CO}_2$ correlations also exhibited similar patterns (Figure 7).

6.2. Impact of Unbalanced In-Situ Measurements Distribution on the Model for $p\text{CO}_2$ Estimate

The in-situ $p\text{CO}_2$ measurements available in the Baltic Sea during 2002–2011 were unevenly distributed, namely, relatively sparse measurements in the north and dense measurements in the south (Figure 1). In order to ensure the participation of the in-

situ data from the northern Baltic Sea, we selected in-situ data month-wise to train and validate the model for pCO₂ estimation, instead of randomly selecting from the in-situ measurements. However, this measure led to the missing determination of variables' importance for the Gulf of Bothnia due to the few months of in-situ measurements in this basin (i.e., March 2006 and September 2009). In the future, including additional in-situ pCO₂ measurements from the Gulf of Bothnia can help analyze the variables' importance for the pCO₂ estimate in that region and understand the processes controlling pCO₂ there. These additional in-situ pCO₂ measurements are also expected to improve the RMSE of pCO₂ estimate for the entire Baltic Sea.

Despite the unbalanced distribution of in-situ data in the Baltic Sea, the monthly pCO₂ maps were retrieved for the Baltic Sea for the period of August–October 2011 (Figure 5). The RMSE of the model for pCO₂ estimation was 47.8 μatm (Figure 4), slightly larger than 25 μatm and 31.7 μatm, the RMSEs of the models constructed by [16] and [17], respectively, for pCO₂ estimation in the Gulf of Mexico using similar tree-based regression algorithms. Still, the RMSE of 47.8 μatm is relatively small for pCO₂ estimation in the Baltic Sea, considering the following factors: (1) the pCO₂ estimation was undertaken on the monthly frequency, where the in-situ data from entire month was integrated to the few days with remote sensing images; (2) The magnitudes of the seasonal changes in pCO₂ in the Baltic Sea are much larger than that in middle or low latitude marginal seas. For example, the pCO₂ in the Baltic Sea was in the range of 100–600 μatm (Figure 8), while, in the Gulf of Mexico, it was 200–450 μatm [16], and, in the South China Sea, it was 250–450 μatm [11]; (3). The processes controlling pCO₂ across the Baltic sea (e.g., phytoplankton photosynthesis, bacteria respiration and runoff) vary spatially and temporally [30,82] and thus increase the difficulties in mapping pCO₂ in the Baltic Sea with high accuracy; (4) Upwelling takes place in the Baltic Sea with varying frequencies among years and months [83] and complicates the pCO₂ process in multiple manners [34,84]. Even though we eliminated the months dominated by upwelling, few upwelling might have remained in the rest of the months and increased the RMSE of the model; (5) Most importantly, the random forest model covered the processes that took place in the entire Baltic Sea in all the seasons in the period of 2002–2011. This task itself is a challenging one due to the above factors. All these factors rendered deriving sea surface pCO₂ in the Baltic Sea more challenging than in other marginal seas.

The random forest algorithm outperformed SOM and MLR in the sea surface pCO₂ estimation (Figure 8). We attributed this to how the three algorithms treated the variables. In random forest, a series of forests were constructed, and the most effective one was chosen for prediction [59,65]. While the variables and training samples were randomly selected for the tree construction, the best model was the one with little participation of the unimportant variables. In contrast, when the mode was constructed with SOM, all the input variables had the same weights [70]. This very likely amplified the contribution of the unimportant or correlated variables and suppresses the important ones at the corresponding temporal and spatial scale, thus caused misestimates (Figure 8A,C). The variants of SOM, such as SOMLO, probably also inherit such effects. MLR attributed weights to the input variables by determining their correlation coefficients to the dependent variables. The effect of the coefficients is very evident in the case when the training samples were chosen across months and cover a large variation. For example, in the experiments in Figure 8A–C, the samples covered 2/3 of the months and performed RMSE similar to that of random forest and better than SOM. In contrast, in the experiment where the samples were 2/3 of the entire in-situ data set from random selection, samples from the same season/months of high similarity were likely used. Given that the time window of in-situ data was narrowed down to 9:00–14:00, and the in-situ data from the months dominated by upwelling were also removed, we did not consider the effect of outlier on the modeling and the errors produced by the models were regarded to be from the misestimate of the models. Overall, random forest performs better than MLR and SOM regardless of the variation range of the training data. MLR performs better than SOM when the training data cover a large

variation, and SOM performs better than MLR when the training data cover a relatively small variation.

6.3. $p\text{CO}_2$ Maps for the Baltic Sea and Its Spatiotemporal Characteristics

In this study, we produced the monthly $p\text{CO}_2$ maps for the entire Baltic Sea over the period of August 2002–October 2020. These maps showed that $p\text{CO}_2$ across the Baltic Sea was characterized by strong seasonality, generally, high $p\text{CO}_2$ in winter and low $p\text{CO}_2$ in summer (Figures 5 and 6). The trend aligned well with that derived from in-situ data in the Baltic Sea [85]. The seasonality of $p\text{CO}_2$ in the Baltic Sea was similar to that in the marginal sea of Gulf of Maine but different from the one observed in Gulf of Mexico by [16]. In addition, the range of seasonal $p\text{CO}_2$ variation in the Baltic Sea (i.e., 100–500 μatm) was larger than that observed for the two marginal seas (i.e., 300–500 μatm) (Figures 5 and 6) [16]. These different seasonal variations trends and variables' importance (e.g., $K_d_{490\text{nm}}$) suggest that the processes determining the $p\text{CO}_2$ in the Baltic Sea are likely different from that observed in other seas, or same processes work on different intensity, for example, the gradient in PAR.

In addition to the similar seasonal trend, minor differences exist in the seasonal trends of $p\text{CO}_2$ in the Baltic Sea. For example, Baltic Proper and the Gulf of Finland showed $p\text{CO}_2$ minima both in May and July, while, in the Bothnia Bay and Bothnia Sea, it was only shown on minima in June (Figure 6). May is the time when most rivers pass their annual peak of water levels [30], and, in July, the daytime is the longest in a year in Baltic Sea, with the most sunny days. In addition, different areas in the Baltic Sea showed interannual variations in different months (Figure 6). For example, the waters in the Gulf of Finland exhibited large interannual variation in April (Figure 6D), when the large river input take place in the sub-basin [27]. The Baltic Proper showed such variations during May–July (Figure 6E), when the primary production is high in this sub-basin and upwelling also occurs very often there [58,68]. This indicates that the dominantly driver of $p\text{CO}_2$ are spatially variable across the Baltic Sea. The $p\text{CO}_2$ maps derived from this model exhibited continuous transitions between the sub-basins of the Baltic Sea (Figure 5). Therefore, these maps are a significant improvement from those produced in previous studied by dividing the Baltic sea into different sub-basins [12].

7. Conclusions

This study analyzed the variables' importance in the $p\text{CO}_2$ estimation for the Baltic Sea across different time and sub-basins with the support of remote sensing and derived $p\text{CO}_2$ maps for the Baltic Sea from August 2002 to October 2011. We found that the contributions of the variables to $p\text{CO}_2$ retrieval for the Baltic Sea vary both spatially and temporally and likely replicated the spatiotemporal characteristics of the driving forces. Among all the variables, PAR was the most important, followed by SST and MLD. Chl-a contributed surprisingly little to the $p\text{CO}_2$ estimate. a_{CDOM} was important for the $p\text{CO}_2$ estimation for the Gulf of Finland and the Gulf of Riga. The random forest model used for the $p\text{CO}_2$ estimate for the entire Baltic Sea had the RMSE of 47.8 μatm , MAE of -3.26 μatm , and coefficient of determination of 0.63. These $p\text{CO}_2$ maps derived in this study are one of the most reliable $p\text{CO}_2$ fields in the Baltic Sea and can potentially support determining the role of the Baltic Sea as sink/source of the atmospheric CO_2 . Moreover, the variables importance/relevance from this study can provide a benchmark for understanding the different drivers of $p\text{CO}_2$ in the Baltic Sea and how they vary in different time and space.

In the Baltic Sea region, frequent clouds in November, December, and January lead to the absence of $p\text{CO}_2$ maps during those three months. This is an inevitable situation considering the high-latitude location of the Baltic Sea. Derivation of sea surface $p\text{CO}_2$ for the Baltic Sea in the wintertime needs to be achieved by combining the remote sensing supported results with additional sources information, e.g., modeling.

Supplementary Materials: The following are available online at <https://www.mdpi.com/2072-4292/13/2/259/s1>, Figure S1: Spatial and temporal distributions of the in-situ data used for training and validating the pCO₂ estimate. Figure S2: Diurnal effect on the pCO₂ estimate. Figure S3: Scenarios where the upwelling affects the pCO₂ estimate from remote sensing images. Figure S4: The effect of upwelling in the pCO₂ estimate with remote sensing image. Figure S5: The monthly mean product of Chl-a derived from MODIS and MERIS images in May, July and September 2011 mapping the Baltic Sea. Figure S6: a_{CDOM} from MODIS and MERIS in the Baltic Sea. Figure S7: The performance differences between of Chl-a from MODIS and Chl-a from MERIS in the pCO₂ estimate. Figure S8: Alternative of the final model for pCO₂ estimate in the entire Baltic Sea. Figure S9: Relationship between variables in the Baltic Sea.

Author Contributions: S.Z., A.R. and P.P. designed the study. S.Z. did the data collection, analysis and manuscript preparation. Writing—review & editing, S.Z., A.R., P.P. and M.B.W. Investigation, S.Z., P.P. and M.B.W. All authors have read and agreed to the published version of the manuscript.

Funding: Swedish National Space Board (Project No: 174/17) and the BONUS Blue Baltic (Call No. 2015-101: Integrated carbon and Trace Gas monitoring for the Baltic sea) funded this study.

Institutional Review Board Statement: Not applicable.

Informed Consent Statement: Informed consent was obtained from all subjects involved in the study.

Data Availability Statement: Not applicable.

Acknowledgments: The computations were performed on Swedish National Infrastructure for Computing (SNIC) through Uppsala Multidisciplinary Center for Advanced Computational Science (UPPMAX) (Project No. SNIC 2019-8-223 & SNIC2019-30-7). The MODIS data were provided by Physical Oceanography Distributed Active Archive Center (PODAAC: <https://podaac.jpl.nasa.gov/>). Copernicus Marine Environment Monitoring Service (CMEMS: <https://marine.copernicus.eu/>) provided SSS and MLD data. The ICOS (Integrated Carbon Observation System) station Östergarnsholm is funded by Swedish Research Council and Uppsala University. Bernd Schneider and Matti Perttilä coordinated in the provision of original data used by Löffler et al. (2012). We are thankful to the constructive comments from three anonymous reviewers.

Conflicts of Interest: The authors declare no conflict of interest.

References

1. Gruber, N.; Clement, D.; Carter, B.R.; Feely, R.A.; Van Heuven, S.; Hoppema, M.; Ishii, M.; Key, R.M.; Kozyr, A.; Lauvset, S.K.; et al. The oceanic sink for anthropogenic CO₂ from 1994 to 2007. *Science* **2019**, *363*, 1193–1199. [[CrossRef](#)]
2. Laruelle, G.G.; Cai, W.; Hu, X.; Gruber, N.; MacKenzie, F.T.; Regnier, P. Continental shelves as a variable but increasing global sink for atmospheric carbon dioxide. *Nat. Commun.* **2018**, *9*, 1–11. [[CrossRef](#)]
3. Gruber, N. Carbon at the coastal interface. *Nat. Cell Biol.* **2015**, *517*, 148–149. [[CrossRef](#)]
4. Laruelle, G.G.; Lauerwald, R.; Pfeil, B.; Regnier, P. Regionalized global budget of the CO₂ exchange at the air-water interface in continental shelf seas. *Glob. Biogeochem. Cycles* **2014**, *28*, 1199–1214. [[CrossRef](#)]
5. Hofmann, E.E.; Cahill, B.; Fennel, K.; Friedrichs, M.A.; Hyde, K.; Lee, C.; Mannino, A.; Najjar, R.G.; O'Reilly, J.E.; Wilkin, J.; et al. Modeling the Dynamics of Continental Shelf Carbon. *Annu. Rev. Mar. Sci.* **2011**, *3*, 93–122. [[CrossRef](#)]
6. Fennel, K.; Wilkin, J.; Previdi, M.; Najjar, R. Denitrification effects on air-sea CO₂ flux in the coastal ocean. *Geophys. Res. Lett.* **2008**, *35*, 1–5. [[CrossRef](#)]
7. Xue, L.; Cai, W.-J.; Hu, X.; Sabine, C.L.; Jones, S.M.; Sutton, A.J.; Jiang, L.-Q.; Reimer, J.J. Sea surface carbon dioxide at the Georgia time series site (2006–2007): Air–sea flux and controlling processes. *Prog. Oceanogr.* **2016**, *140*, 14–26. [[CrossRef](#)]
8. Schneider, B.; Müller, J.D. *Biogeochemical Transformations in the Baltic Sea—Observations through Carbon Dioxide Glasses*; Springer: Berlin/Heidelberg, Germany, 2018; ISBN 978-3-319-61698-8.
9. Chierici, M.; Signorini, S.R.; Mattsdotter-Björk, M.; Fransson, A.; Olsen, A. Surface water fCO₂ algorithms for the high-latitude Pacific sector of the Southern Ocean. *Remote Sens. Environ.* **2012**, *119*, 184–196. [[CrossRef](#)]
10. Chen, S.; Hu, C.; Cai, W.; Yang, B. Estimating surface pCO₂ in the northern Gulf of Mexico: Which remote sensing model to use? *Cont. Shelf Res.* **2017**, *151*, 94–110. [[CrossRef](#)]
11. Jo, Y.-H.; Dai, M.; Zhai, W.; Yan, X.-H.; Shang, S. On the variations of sea surface pCO₂ in the northern South China Sea: A remote sensing based neural network approach. *J. Geophys. Res. Space Phys.* **2012**, *117*, 1–13. [[CrossRef](#)]
12. Parard, G.; Charantonis, A.A.; Rutgersson, A. Remote sensing the sea surface CO₂ of the Baltic Sea using the SOMLO methodology. *Biogeosciences* **2015**, *12*, 3369–3384. [[CrossRef](#)]
13. Fay, A.R.; McKinley, G. Correlations of surface ocean pCO₂ to satellite chlorophyll on monthly to interannual timescales. *Glob. Biogeochem. Cycles* **2017**, *31*, 436–455. [[CrossRef](#)]

14. Gustafsson, E.; Omstedt, A.; Gustafsson, B.G. The air-water CO₂ exchange of a coastal sea—A sensitivity study on factors that influence the absorption and outgassing of CO₂ in the Baltic Sea. *J. Geophys. Res. Oceans* **2015**, *120*, 5342–5357. [[CrossRef](#)]
15. Gustafsson, E.; Deutsch, B.; Gustafsson, B.; Humborg, C.; Mörth, C.-M. Carbon cycling in the Baltic Sea—The fate of allochthonous organic carbon and its impact on air–sea CO₂ exchange. *J. Mar. Syst.* **2014**, *129*, 289–302. [[CrossRef](#)]
16. Chen, S.; Hu, C.; Barnes, B.B.; Wanninkhof, R.; Cai, W.-J.; Barbero, L.; Pierrot, D. A machine learning approach to estimate surface ocean pCO₂ from satellite measurements. *Remote Sens. Environ.* **2019**, *228*, 203–226. [[CrossRef](#)]
17. Lohrenz, S.E.; Cai, W.; Chakraborty, S.; Huang, W.-J.; Guo, X.; He, R.; Xue, Z.G.; Fennel, K.; Howden, S.; Tian, H. Satellite estimation of coastal pCO₂ and air-sea flux of carbon dioxide in the northern Gulf of Mexico. *Remote Sens. Environ.* **2018**, *207*, 71–83. [[CrossRef](#)]
18. Ikawa, H.; Faloon, I.; Kochendorfer, J.; Paw, K.T.; Oechel, W. Air–sea exchange of CO₂ at a Northern California coastal site along the California Current upwelling system. *Biogeosciences* **2013**, *10*, 4419–4432. [[CrossRef](#)]
19. Joshi, I.D.; Ward, N.D.; D’Sa, E.J.; Osburn, C.L.; Bianchi, T.S.; Oviedo-Vargas, D. Seasonal Trends in Surface pCO₂ and Air-Sea CO₂ Fluxes in Apalachicola Bay, Florida, From VIIRS Ocean Color. *J. Geophys. Res. Biogeosci.* **2018**, *123*, 2466–2484. [[CrossRef](#)]
20. Telszewski, M.; Chazottes, A.; Schuster, U.; Watson, A.J.; Moulin, C.; Bakker, D.C.E.; González-Dávila, M.; Johannessen, T.; Körtzinger, A.; Lüger, H.; et al. Estimating the monthly pCO₂ distribution in the North Atlantic using a self-organizing neural network. *Biogeosciences* **2009**, *6*, 1405–1421. [[CrossRef](#)]
21. Friedrich, T.; Oeschler, A. Neural network-based estimates of North Atlantic surface pCO₂ from satellite data: A methodological study. *J. Geophys. Res. Space Phys.* **2009**, *114*, 1–12. [[CrossRef](#)]
22. Hales, B.; Strutton, P.G.; Saraceno, M.; Letelier, R.; Takahashi, T.; Feely, R.; Sabine, C.; Chavez, F. Satellite-based prediction of pCO₂ in coastal waters of the eastern North Pacific. *Prog. Oceanogr.* **2012**, *103*, 1–15. [[CrossRef](#)]
23. Salisbury, J.; VanDeMark, D.; Hunt, C.W.; Campbell, J.W.; McGillis, W.R.; McDowell, W.H. Seasonal observations of surface waters in two Gulf of Maine estuary-plume systems: Relationships between watershed attributes, optical measurements and surface pCO₂. *Estuar. Coast. Shelf Sci.* **2008**, *77*, 245–252. [[CrossRef](#)]
24. Signorini, S.R.; Mannino, A.; Najjar, R.G., Jr.; Friedrichs, M.A.M.; Cai, W.-J.; Salisbury, J.; Wang, Z.A.; Thomas, H.; Shadwick, E.H. Surface ocean pCO₂ seasonality and sea-air CO₂ flux estimates for the North American east coast. *J. Geophys. Res. Oceans* **2013**, *118*, 5439–5460. [[CrossRef](#)]
25. Bai, Y.; Cai, W.-J.; He, X.; Zhai, W.; Pan, D.; Dai, M.; Yu, P. A mechanistic semi-analytical method for remotely sensing sea surface pCO₂ in river-dominated coastal oceans: A case study from the East China Sea. *J. Geophys. Res. Oceans* **2015**, *120*, 2331–2349. [[CrossRef](#)]
26. Song, X.; Bai, Y.; Cai, W.; Chen, C.-T.A.; Pan, D.; He, X.; Zhu, Q. Remote Sensing of Sea Surface pCO₂ in the Bering Sea in Summer Based on a Mechanistic Semi-Analytical Algorithm (MeSAA). *Remote Sens.* **2016**, *8*, 558. [[CrossRef](#)]
27. Bergström, S.; Carlsson, B. River runoff to the Baltic Sea. *Ambio* **1994**, *23*, 280–287.
28. Omstedt, A.; Elken, J.; Lehmann, A.D.; Piechura, J. Knowledge of the Baltic Sea physics gained during the BALTEX and related programmes. *Prog. Oceanogr.* **2004**, *63*, 1–28. [[CrossRef](#)]
29. Meier, H.E.M.; Rutgersson, A.; Reckermann, M. An Earth System Science Program for the Baltic Sea Region. *Eos* **2014**, *95*, 109–110. [[CrossRef](#)]
30. Käyhkö, J.; Apsite, E.; Bolek, A.; Filatov, N.; Kondratyev, S.; Korhonen, J.; Kriaučiūnienė, J.; Lindström, G.; Nazarova, L.; Pyrh, A.; et al. Recent Change—River Run-off and Ice Cover. In *Second Assessment of Climate Change for the Baltic Sea Basin*; Regional Climate Studies Series; Springer: Berlin/Heidelberg, Germany, 2015; pp. 99–115. ISBN 9783319160054.
31. Schneider, B.; Dellwig, O.; Kuliński, K.; Omstedt, A.; Pollehne, F.; Rehder, G.; Savchuk, O. Ecological processes in the Baltic Sea. In *Biological Oceanography of the Baltic Sea*; Snoeijs-Leijonmalm, P., Schubert, H., Radziejewska, T., Eds.; Springer Nature: Berlin/Heidelberg, Germany, 2017; Volume 30, pp. 87–278. ISBN 9789400706675.
32. Lehmann, A.; Myrberg, K. Upwelling in the Baltic Sea—A review. *J. Mar. Syst.* **2008**, *74*, S3–S12. [[CrossRef](#)]
33. Norman, M.; Parampil, S.R.; Rutgersson, A.; Sahlée, E. Influence of coastal upwelling on the air–sea gas exchange of CO₂ in a Baltic Sea Basin. *Tellus B Chem. Phys. Meteorol.* **2013**, *65*, 1–16. [[CrossRef](#)]
34. Wasmund, N.; Nausch, G.; Voss, M. Upwelling events may cause cyanobacteria blooms in the Baltic Sea. *J. Mar. Syst.* **2012**, *90*, 67–76. [[CrossRef](#)]
35. Wesslander, K.; Hall, P.; Hjalmarsson, S.; Lefèvre, M.; Omstedt, A.; Rutgersson, A.; Sahlée, E.; Tengberg, A. Observed carbon dioxide and oxygen dynamics in a Baltic Sea coastal region. *J. Mar. Syst.* **2011**, *86*, 1–9. [[CrossRef](#)]
36. Barnes, B.B.; Hu, C.; Schaeffer, B.A.; Lee, Z.; Palandro, D.; Lehrter, J.C. MODIS-derived spatiotemporal water clarity patterns in optically shallow Florida Keys waters: A new approach to remove bottom contamination. *Remote Sens. Environ.* **2013**, *134*, 377–391. [[CrossRef](#)]
37. Hu, C.; Muller-Karger, F.E.; Taylor, C.J.; Carder, K.L.; Kelble, C.; Johns, E.; Heil, C.A. Red tide detection and tracing using MODIS fluorescence data: A regional example in SW Florida coastal waters. *Remote Sens. Environ.* **2005**, *97*, 311–321. [[CrossRef](#)]
38. Shi, K.; Zhang, Y.; Zhu, G.; Liu, X.; Zhou, Y.; Xu, H.; Qin, B.; Liu, G.; Li, Y. Long-term remote monitoring of total suspended matter concentration in Lake Taihu using 250 m MODIS-Aqua data. *Remote Sens. Environ.* **2015**, *164*, 43–56. [[CrossRef](#)]
39. Liu, B.; D’Sa, E.J.; Joshi, I.D. Multi-decadal trends and influences on dissolved organic carbon distribution in the Barataria Basin, Louisiana from in-situ and Landsat/MODIS observations. *Remote Sens. Environ.* **2019**, *228*, 183–202. [[CrossRef](#)]

40. Parard, G.; Charantonis, A.; Rutgersson, A. Using satellite data to estimate partial pressure of CO₂ in the Baltic Sea. *J. Geophys. Res. Biogeosci.* **2016**, *121*, 1002–1015. [[CrossRef](#)]
41. Chen, S.; Hu, C.; Byrne, R.H.; Robbins, L.L.; Yang, B. Remote estimation of surface pCO₂ on the West Florida Shelf. *Cont. Shelf Res.* **2016**, *128*, 10–25. [[CrossRef](#)]
42. Gower, J.; King, S. Satellite Images Show the Movement of Floating Sargassum in the Gulf of Mexico and Atlantic Ocean. *Nat. Preced.* **2008**, 1–13. [[CrossRef](#)]
43. Gower, J.; King, S.; Borstad, G.; Brown, L. Detection of intense plankton blooms using the 709 nm band of the MERIS imaging spectrometer. *Int. J. Remote Sens.* **2005**, *26*, 2005–2012. [[CrossRef](#)]
44. Matthews, M.W. Eutrophication and cyanobacterial blooms in South African inland waters: 10 years of MERIS observations. *Remote Sens. Environ.* **2014**, *155*, 161–177. [[CrossRef](#)]
45. Attila, J.; Kauppila, P.; Kallio, K.Y.; Alasalmi, H.; Keto, V.; Bruun, E.; Koponen, S. Applicability of Earth Observation chlorophyll-a data in assessment of water status via MERIS—With implications for the use of OLCI sensors. *Remote Sens. Environ.* **2018**, *212*, 273–287. [[CrossRef](#)]
46. Vilas, L.G.; Spyarakos, E.; Palenzuela, J.M.T. Neural network estimation of chlorophyll a from MERIS full resolution data for the coastal waters of Galician rias (NW Spain). *Remote Sens. Environ.* **2011**, *115*, 524–535. [[CrossRef](#)]
47. Loisel, H.; Mangin, A.; Vantrepotte, V.; Dessailly, D.; Dinh, D.N.; Garnesson, P.; Ouillon, S.; Lefebvre, J.-P.; Mériaux, X.; Phan, T.M. Variability of suspended particulate matter concentration in coastal waters under the Mekong’s influence from ocean color (MERIS) remote sensing over the last decade. *Remote Sens. Environ.* **2014**, *150*, 218–230. [[CrossRef](#)]
48. Kutser, T.; Verpoorter, C.; Paavel, B.; Tranvik, L.J. Estimating lake carbon fractions from remote sensing data. *Remote Sens. Environ.* **2015**, *157*, 138–146. [[CrossRef](#)]
49. Kratzer, S.; Brockmann, C.; Moore, G. Using MERIS full resolution data to monitor coastal waters—A case study from Himmerfjärden, a fjord-like bay in the northwestern Baltic Sea. *Remote Sens. Environ.* **2008**, *112*, 2284–2300. [[CrossRef](#)]
50. Schroeder, T.; Schaale, M.; Fischer, J. Retrieval of atmospheric and oceanic properties from MERIS measurements: A new Case-2 water processor for BEAM. *Int. J. Remote Sens.* **2007**, *28*, 5627–5632. [[CrossRef](#)]
51. Olsen, A.; Brown, K.R.; Chierici, M.; Johannessen, T.; Neill, C.J. Sea-surface CO₂ fugacity in the subpolar North Atlantic. *Biogeosciences* **2008**, *5*, 535–547. [[CrossRef](#)]
52. Chierici, M.; Olsen, A.; Johannessen, T.; Trinañes, J.; Wanninkhof, R. Algorithms to estimate the carbon dioxide uptake in the northern North Atlantic using shipboard observations, satellite and ocean analysis data. *Deep Sea Res. Part II Top. Stud. Oceanogr.* **2009**, *56*, 630–639. [[CrossRef](#)]
53. Axell, L. *CMEMS Baltic Sea Physical Reanalysis Product BALTICSEA_REANALYSIS_PHY_003_011*; EU Copernicus Marine Service: Toulouse, France, 2019.
54. Bakker, D.C.E.; Pfeil, B.; Landa, C.S.; Metzl, N.; O’Brien, K.M.; Olsen, A.; Smith, K.; Cosca, C.; Harasawa, S.; Jones, S.D.; et al. A multi-decade record of high-quality fCO₂ data in version 3 of the Surface Ocean CO₂ Atlas (SOCAT). *Earth Syst. Sci. Data* **2016**, *8*, 383–413. [[CrossRef](#)]
55. Rutgersson, A.; Pettersson, H.; Nilsson, E.; Bergström, H.; Wallin, M.B.; Sahlée, E.; Wu, L.E.; Mårtensson, E.M. Using land-based stations for air–sea interaction studies. *Tellus A Dyn. Meteorol. Oceanogr.* **2019**, *72*, 1–23. [[CrossRef](#)]
56. Löffler, A.; Schneider, B.; Perttilä, M.; Rehder, G. Air–sea CO₂ exchange in the Gulf of Bothnia, Baltic Sea. *Cont. Shelf Res.* **2012**, *37*, 46–56. [[CrossRef](#)]
57. Pfeil, B.; Olsen, A.; Bakker, D.C.E.; Hankin, S.; Koyuk, H.; Kozyr, A.; Malczyk, J.; Manke, A.; Metzl, N.; Sabine, C.L.; et al. A uniform, quality controlled Surface Ocean CO₂ Atlas (SOCAT). *Earth Syst. Sci. Data* **2013**, *5*, 125–143. [[CrossRef](#)]
58. Schneider, B.; Kaitala, S.; Maunula, P. Identification and quantification of plankton bloom events in the Baltic Sea by continuous pCO₂ and chlorophyll a measurements on a cargo ship. *J. Mar. Syst.* **2006**, *59*, 238–248. [[CrossRef](#)]
59. Breiman, L. *Random Forest*; University of California Berkeley: Berkeley, CA, USA, 2001.
60. Belgiu, M.; Drăgut, L. Random forest in remote sensing: A review of applications and future directions. *ISPRS J. Photogramm. Remote Sens.* **2016**, *114*, 24–31. [[CrossRef](#)]
61. Waske, B.; Member, A.; Van Der Linden, S. Classifying Multilevel Imagery from SAR and Optical Sensors by Decision Fusion. *IEEE Trans. Geosci. Remote Sens.* **2008**, *46*, 1457–1466. [[CrossRef](#)]
62. Wolanin, A.; Camps-Valls, G.; Gómez-Chova, L.; Mateo-García, G.; Van Der Tol, C.; Zhang, Y.; Guanter, L. Estimating crop primary productivity with Sentinel-2 and Landsat 8 using machine learning methods trained with radiative transfer simulations. *Remote Sens. Environ.* **2019**, *225*, 441–457. [[CrossRef](#)]
63. Wei, Z.; Meng, Y.; Zhang, W.; Peng, J.; Meng, L. Downscaling SMAP soil moisture estimation with gradient boosting decision tree regression over the Tibetan Plateau. *Remote Sens. Environ.* **2019**, *225*, 30–44. [[CrossRef](#)]
64. Liu, X.; Guanter, L.; Liu, L.; Damm, A.; Malenovsky, Z.; Rascher, U.; Peng, D.; Du, S.; Gastellu-Etchegorry, J.-P. Downscaling of solar-induced chlorophyll fluorescence from canopy level to photosystem level using a random forest model. *Remote Sens. Environ.* **2019**, *231*, 110772. [[CrossRef](#)]
65. Breiman, L. Bagging predictions. *Mach. Learn.* **1996**, *24*, 123–140. [[CrossRef](#)]
66. Liaw, A.; Wiener, M. Breiman and Cutler’s Random Forests for Classification and Regression; R Package Version: 4.6–14. 2018. Available online: <https://www.stat.berkeley.edu/~breiman/RandomForests/> (accessed on 10 November 2020).

67. R Core Team. *R: A Language and Environment for Statistical Computing*; R Foundation for Statistical Computing: Vienna, Austria, 2018. Available online: <https://www.R-project.org/> (accessed on 10 November 2020).
68. Wesslander, K. *The Carbon Dioxide System in the Baltic Sea Surface Waters*; University of Gotenburg: Gothenburg, Sweden, 2011.
69. Bozec, Y.; Merlivat, L.; Baudoux, A.-C.; De Beaumont, L.; Blain, S.; Bucciarelli, E.; Danguy, T.; Grossteffan, E.; Guillot, A.; Guillou, J.; et al. Diurnal to inter-annual dynamics of pCO₂ recorded by a CARIOCA sensor in a temperate coastal ecosystem (2003–2009). *Mar. Chem.* **2011**, *126*, 13–26. [[CrossRef](#)]
70. Kohonen, T. *Self-Organization and Associative Memory*, 3rd ed.; Huang, T.S., Kohonen, T., Schroeder, M.R., Eds.; Springer: Berlin/Heidelberg, Germany; New York, NY, USA; London, UK; Paris, France; Tokyo, Japan; Hong Kong, China, 2001; ISBN 9783540513872.
71. Landschützer, P.; Gruber, N.; Bakker, D.C.E.; Schuster, U.; Nakaoka, S.; Payne, M.R.; Sasse, T.P.; Zeng, J. A neural network-based estimate of the seasonal to inter-annual variability of the Atlantic Ocean carbon sink. *Biogeosciences* **2013**, *10*, 7793–7815. [[CrossRef](#)]
72. Le Quééré, C.; Moriarty, R.; Andrew, R.M.; Canadell, J.G.; Sitch, S.; Korsbakken, J.L.; Friedlingstein, P.; Peters, G.P.; Andres, R.J.; Boden, T.A.; et al. Global Carbon Budget. *Earth Syst. Sci. Data* **2015**, *7*, 349–396. [[CrossRef](#)]
73. Landschützer, P.; Laruelle, G.G.; Roobaert, A.; Regnier, P. A uniform pCO₂ climatology combining open and coastal oceans. *Earth Syst. Sci. Data* **2020**, *12*, 2537–2553. [[CrossRef](#)]
74. Yasunaka, S.; Siswanto, E.; Olsen, A.; Hoppema, M.; Watanabe, E.; Fransson, A.; Chierici, M.; Murata, A.; Lauvset, S.K.; Wanninkhof, R.; et al. Arctic Ocean CO₂ uptake: An improved multiyear estimate of the air–sea CO₂ flux incorporating chlorophyll a concentrations. *Biogeosciences* **2018**, *15*, 1643–1661. [[CrossRef](#)]
75. Wehrens, R.; Kruisselbrink, J. Flexible Self-Organizing Maps in kohonen 3.0. *J. Stat. Softw.* **2018**, *87*, 1–18. [[CrossRef](#)]
76. Croft, H.; Chen, J.; Wang, R.; Mo, G.; Luo, S.; Luo, X.; He, L.; Gonsamo, A.; Arabian, J.; Zhang, Y.; et al. The global distribution of leaf chlorophyll content. *Remote Sens. Environ.* **2020**, *236*, 111479. [[CrossRef](#)]
77. Haapala, J.J.; Ronkainen, I.; Schmelzer, N.; Sztobryn, M. Recent Change—Sea Ice. In *Second Assessment of Climate Change for the Baltic Sea Basin*; Springer: Berlin/Heidelberg, Germany, 2015; pp. 145–153.
78. Myrberg, K.; Andrejev, O. Main upwelling regions in the Baltic Sea—A statistical analysis based on three-dimensional modelling. *Boreal Environ. Res.* **2003**, *8*, 97–112.
79. Pierson, D.C.; Kratzer, S.; Strömbeck, N.; Håkansson, B. Relationship between the attenuation of downwelling irradiance at 490 nm with the attenuation of PAR (400–700 nm) in the Baltic Sea. *Remote Sens. Environ.* **2008**, *112*, 668–680. [[CrossRef](#)]
80. Stramska, M.; Stramski, D.; Mitchell, B.G.; Mobley, C.D. Estimation of the absorption and backscattering coefficients from in-water radiometric measurements. *Limnol. Oceanogr.* **2000**, *45*, 628–641. [[CrossRef](#)]
81. Stramska, M.; Świrgoń, M. Influence of atmospheric forcing and freshwater discharge on interannual variability of the vertical diffuse attenuation coefficient at 490 nm in the Baltic Sea. *Remote Sens. Environ.* **2014**, *140*, 155–164. [[CrossRef](#)]
82. Algesten, G.; Wikner, J.; Sobek, S.; Tranvik, L.J.; Jansson, M. Seasonal variation of CO₂ saturation in the Gulf of Bothnia: Indications of marine net heterotrophy. *Glob. Biogeochem. Cycles* **2004**, *18*, 1–7. [[CrossRef](#)]
83. Lehmann, A.D.; Myrberg, K.; Höflich, K. A statistical approach to coastal upwelling in the Baltic Sea based on the analysis of satellite data for 1990–2009. *Oceanologia* **2012**, *54*, 369–393. [[CrossRef](#)]
84. Lips, I.; Lips, U.; Liblik, T. Consequences of coastal upwelling events on physical and chemical patterns in the central Gulf of Finland (Baltic Sea). *Cont. Shelf Res.* **2009**, *29*, 1836–1847. [[CrossRef](#)]
85. Wesslander, K.; Omstedt, A.; Schneider, B. Inter-annual and seasonal variations in the air–sea CO₂ balance in the central Baltic Sea and the Kattegat. *Cont. Shelf Res.* **2010**, *30*, 1511–1521. [[CrossRef](#)]